Imaging Earth's Interior based on Spectral-Element and Adjoint Methods

Jeroen Tromp

Hejun Zhu, Ebru Bozdağ, Daniel Peter & Tom Duffy

2010 QUEST Kick Off Meeting

A European model based on full waveform inversion

Imaging & Inversion Challenges

- Cheap, abundant sensors
- Massive amounts of data
  - Industry data sets
  - Regional & global seismology data sets
  - Cross-correlation data sets for interferometry
- On HPC systems, I/O is the bottleneck
- Adopt new data formats for fast parallel I/O
- Data culling tools to reduce preprocessing time
- A standard for the exchange of Earth models
- Adopt workflow management tools
- Data mining, feature extraction, visualization & virtualization

Misfit Function Choices

Waveform differences: $$\chi = \frac{1}{2}\int \left[\mathbf{s}(t,\mathbf{m}) - \mathbf{d}(t)\right]^2 \mathrm{d}t$$

Frequency-dependent phase: $$\chi^{\phi} = \frac{1}{2}\int w_m \left[\frac{\Delta\tau_m(\omega)}{\sigma_m^{\phi}(\omega)}\right]^2 \mathrm{d}\omega$$

Frequency-dependent amplitude: $$\chi^{A} = \frac{1}{2}\int w_m \left[\frac{\Delta \ln A_m(\omega)}{\sigma_m^{A}(\omega)}\right]^2 \mathrm{d}\omega$$

Optimization

Choose misfit function, e.g., $\chi(\mathbf{m}) = \frac{1}{2}\int [\mathbf{s}(t,\mathbf{m}) - \mathbf{d}(t)]^2 \mathrm{dt}$

Taylor expansion: $\chi(\mathbf{m} + \Delta\mathbf{m}) = \chi(\mathbf{m}) + \mathbf{g}(\mathbf{m})\Delta\mathbf{m} + \frac{1}{2}\Delta\mathbf{m}^T\mathbf{H}(\mathbf{m})\Delta\mathbf{m}$

Model update: $\mathbf{H}(\mathbf{m})\Delta\mathbf{m} = -\mathbf{g}(\mathbf{m})$

Steepest descent: $\Delta\mathbf{m} = -\lambda\mathbf{g}(\mathbf{m})$

Optimization:

- Preconditioned conjugate gradient method
- L-BFGS quasi-Newton method

Gradient Calculation: Adjoint Method

Change in Misfit: $\delta\chi = \int_V K_m(\mathbf{x})\delta \ln m(\mathbf{x})\, d^3\mathbf{x}$

Density gradient:

$$K_\rho(\mathbf{x}) = -\int_0^T \rho(\mathbf{x})\mathbf{s}^\dagger(\mathbf{x}, T-t)\cdot\partial_t^2\mathbf{s}(\mathbf{x}, t)\, dt$$

Elastic tensor gradient:

$$K_{c_{jklm}}(\mathbf{x}) = -\int_0^T \epsilon_{jk}^\dagger(\mathbf{x}, T-t)c_{jklm}(\mathbf{x})\epsilon_{lm}(\mathbf{x}, t)\, dt$$

Source of the adjoint wavefield:

$$\mathbf{f}^\dagger(\mathbf{x}, t) = \sum_{r=1}^N [\mathbf{s}(\mathbf{x}_r, T-t) - \mathbf{d}(\mathbf{x}_r, T-t)]\delta(\mathbf{x}-\mathbf{x}_r)$$

The same solver determines the forward and adjoint wavefields!

Adjoint Tomography of Europe

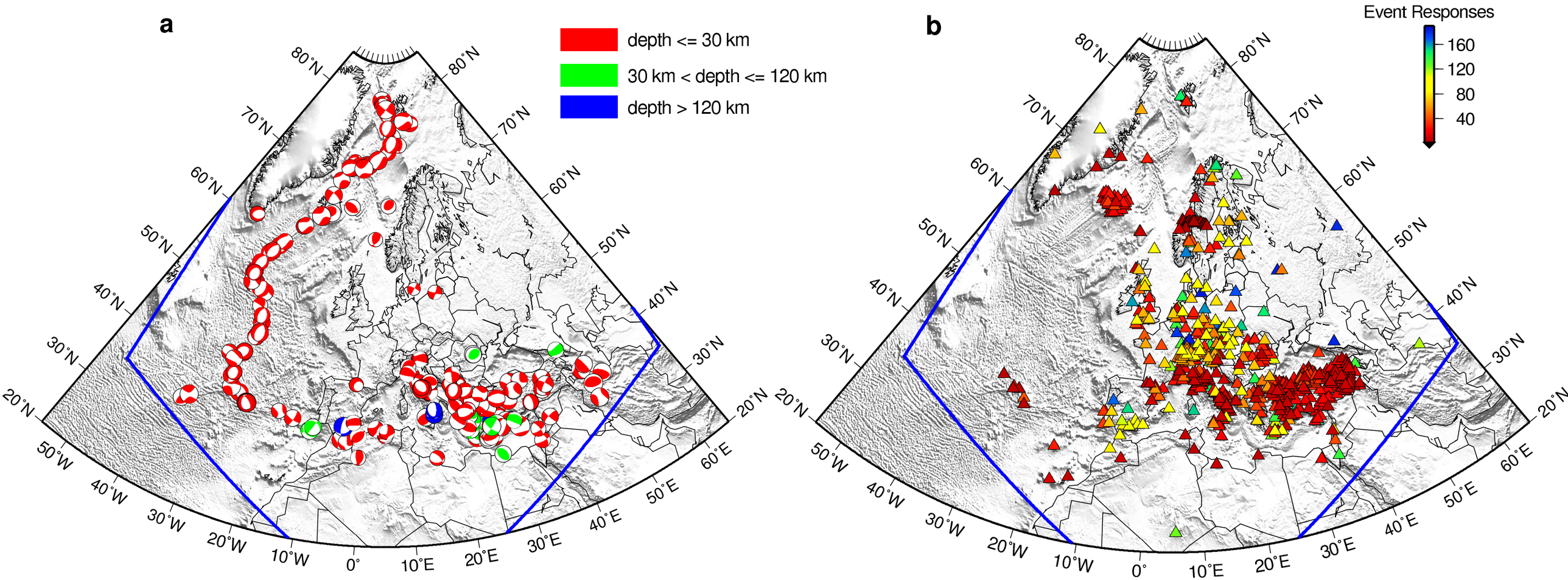

earthquakes	stations	iterations	simulations	CPU hours	measurements
190	745	30	17,100	2.3 million	123,205

Hejun Zhu

IU.KIEV

DIST: 29.37
BCAZ: 316.05
EVDP: 8.70
EVLO: −21.17
EVLA: 63.93
STLO: 29.22
STLA: 50.70
MB: 6.0

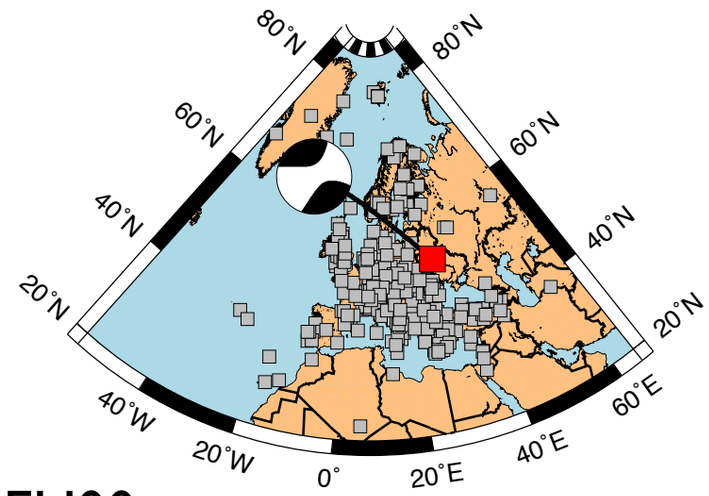

EU00

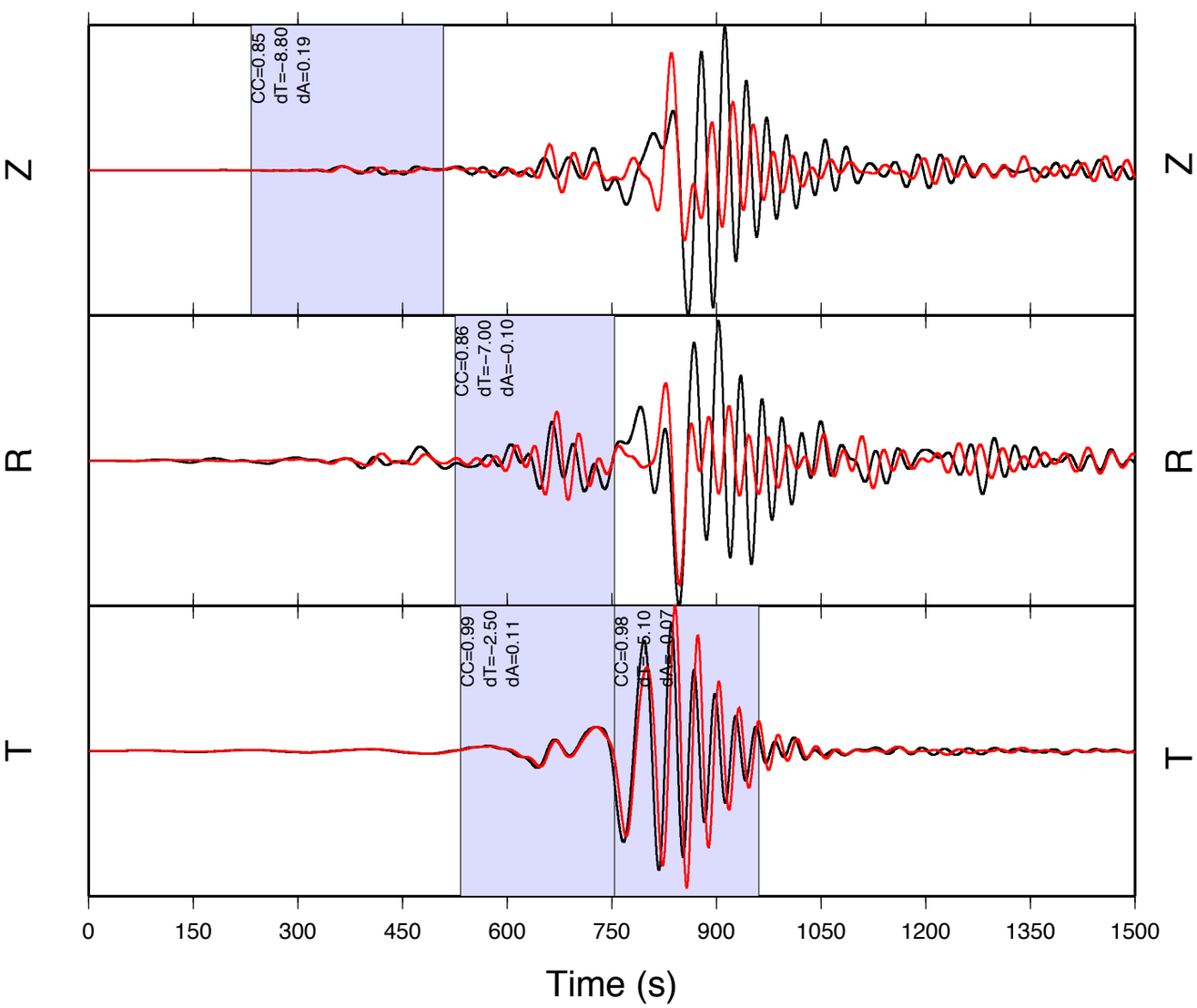

200805291546A

Goal: “Full Waveform Inversion”

Fitting frequency-dependent phase and amplitude anomalies in targeted windows

automated window selection:
FLEXWIN (Maggi et al. 2009)

Stage I. Elastic Inversion

Elastic Misfit Function

Total misfit: $$\chi = \chi^{\phi}$$

Phase misfit: $$\chi^{\phi} = \sum_{c=1}^{N_c} w_c \sum_{m=1}^{N_m} \int w_m \left[\frac{\Delta\tau_m(\omega)}{\sigma_m^{\phi}(\omega)} \right]^2 \mathrm{d}\omega$$

6 Contributions:

- P-SV waves (vertical)
- P-SV waves (radial)
- SH waves (transverse)
- Rayleigh waves (vertical)
- Rayleigh waves (radial)
- Love waves (transverse)

Change in misfit:

$$\delta\chi = \int_{\mathrm{V}} \mathrm{K}_{\beta_{\mathrm{v}}}\, \delta \ln \beta_{\mathrm{v}} + \mathrm{K}_{\beta_{\mathrm{h}}}\, \delta \ln \beta_{\mathrm{h}} + \mathrm{K}_c\, \delta \ln c + \mathrm{K}_{\eta}\, \delta \ln \eta \, \mathrm{d}^3\mathbf{x}$$

Depth 75 km

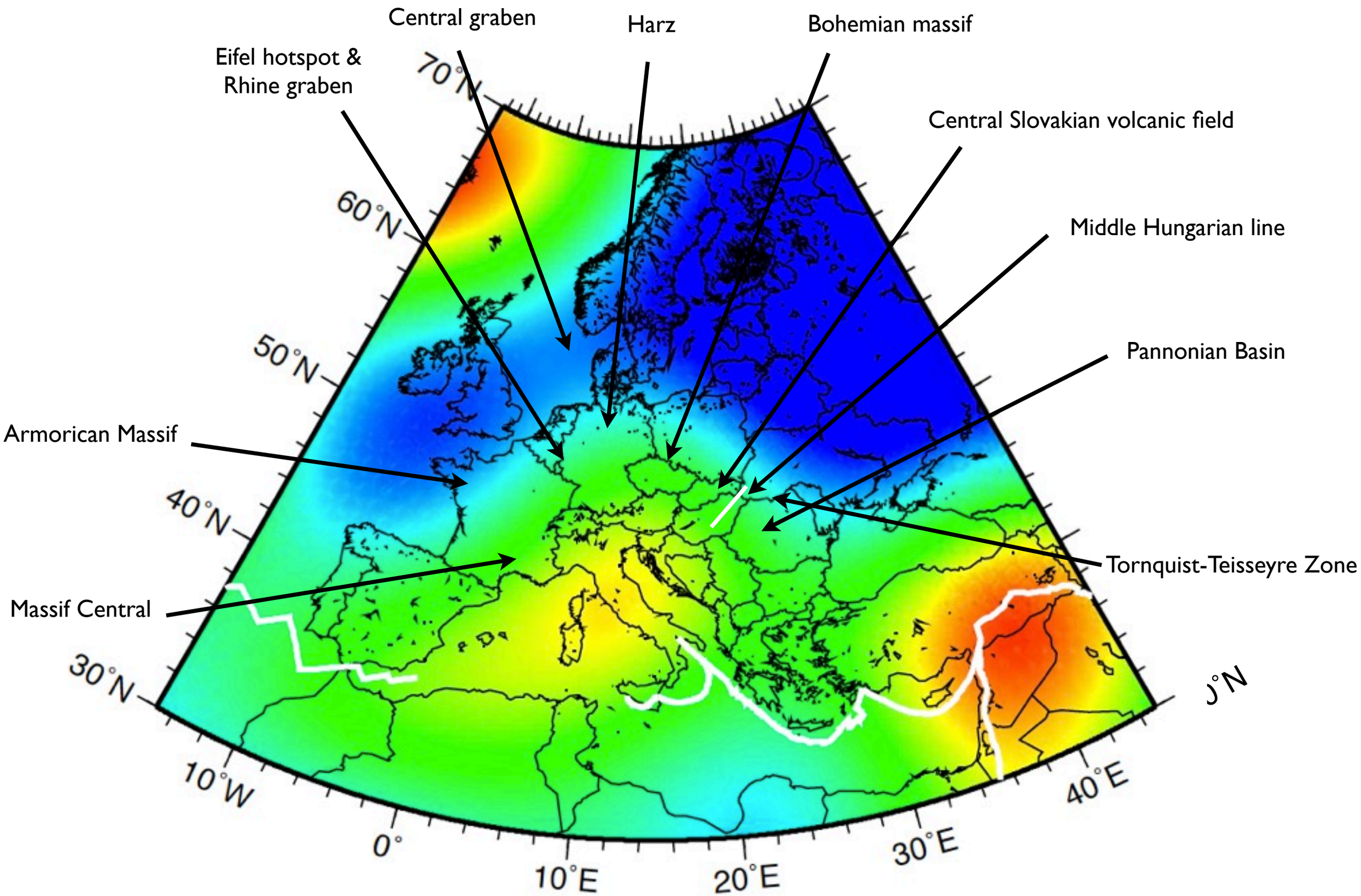
Central graben
Harz
Bohemian massif
Eifel hotspot &
Rhine graben
Central Slovakian volcanic field
Middle Hungarian line
Pannonian Basin
Armorican Massif
Tornquist-Teisseyre Zone
Massif Central
70°N
60°N
50°N
40°N
30°N
10°W
0°
10°E
20°E
30°E
40°E

Adjoint Tomography Workflow

Current data formats are inadequate for fast, parallel I/O

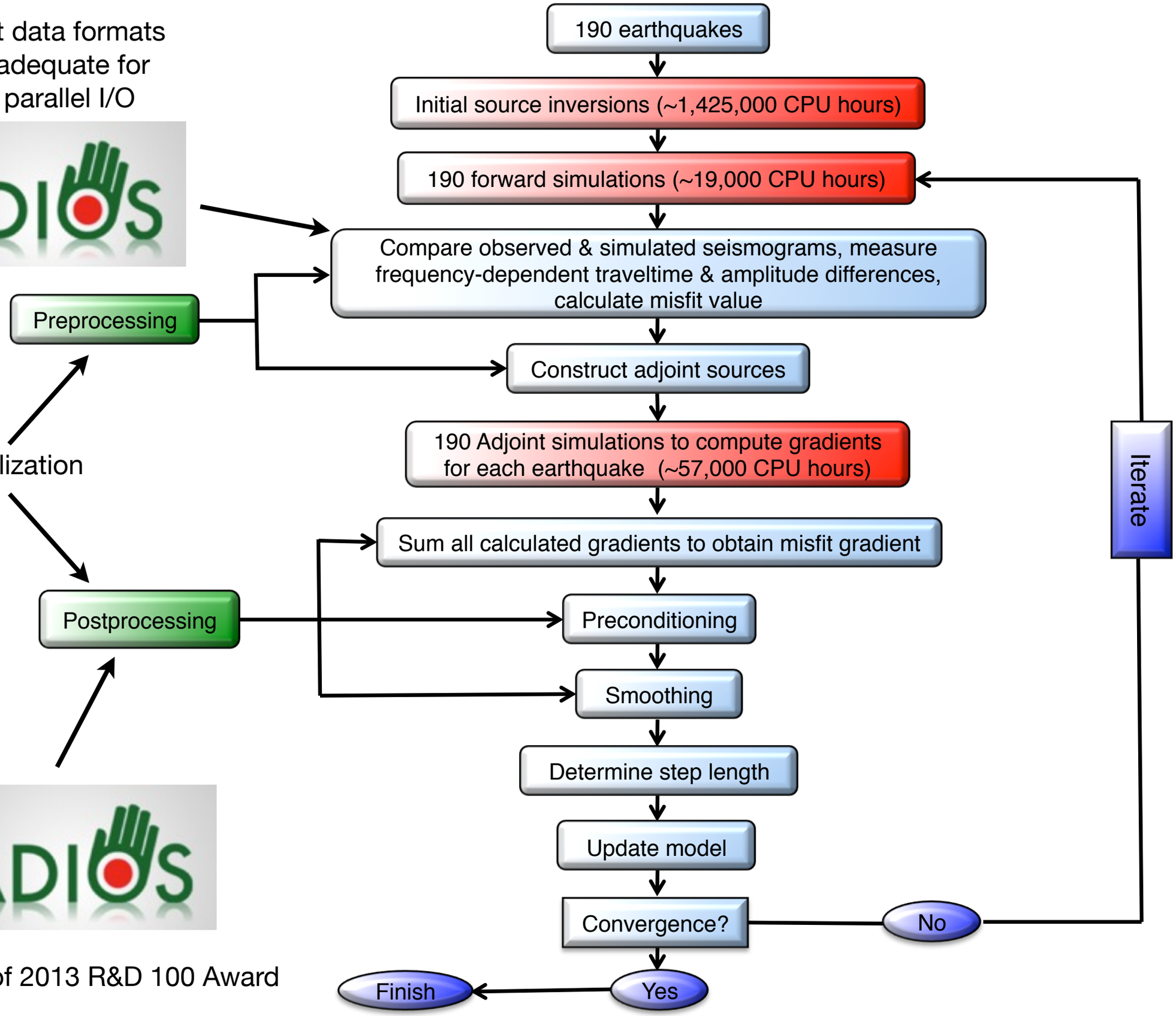

Virtualization

L-BFGS
Quasi-Newton

Winner of 2013 R&D 100 Award

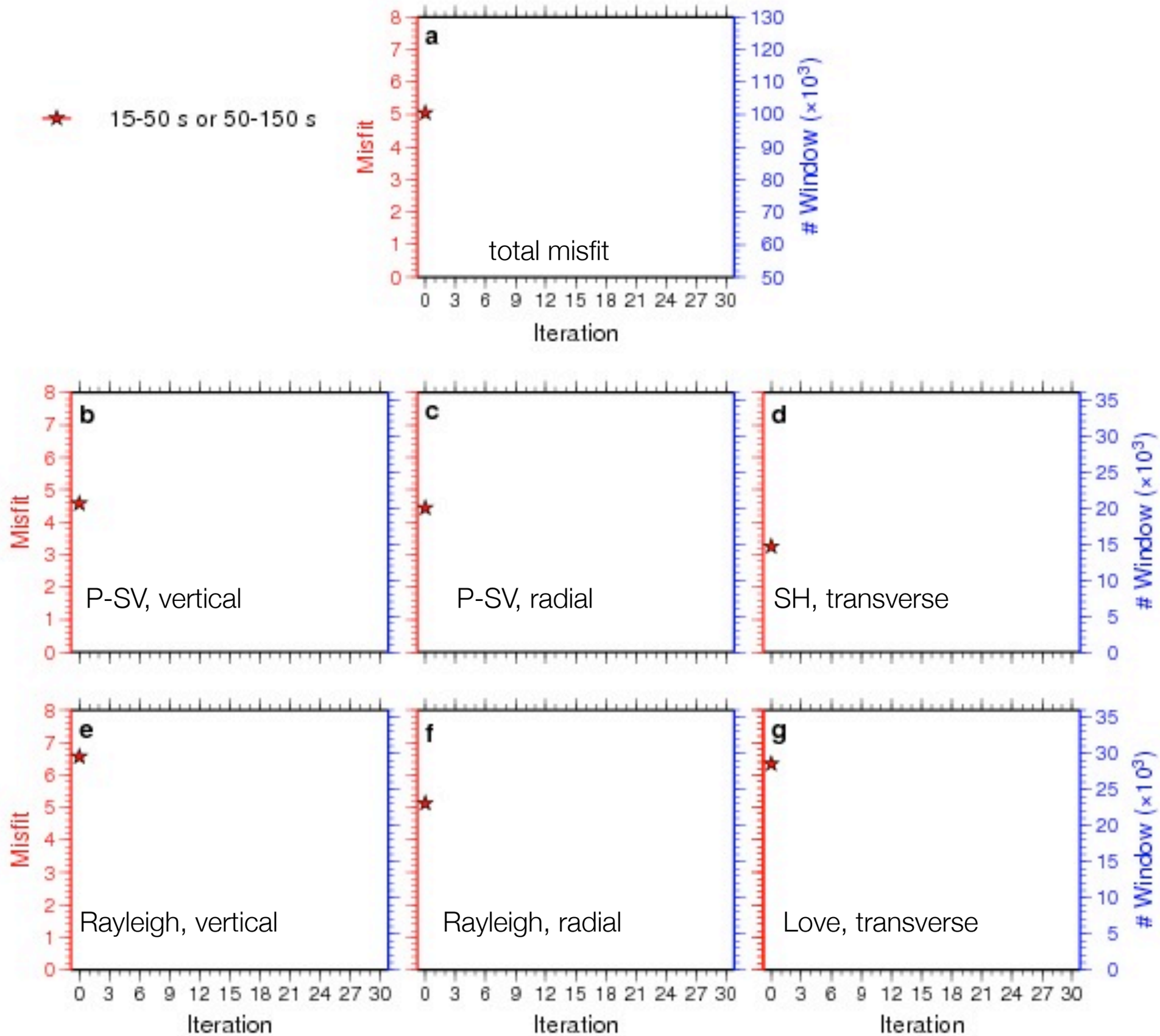
15-50 s or 50-150 s
a
total misfit
Misfit
Window (×10³)
Iteration
b
P-SV, vertical
c
P-SV, radial
d
SH, transverse
e
Rayleigh, vertical
f
Rayleigh, radial
g
Love, transverse

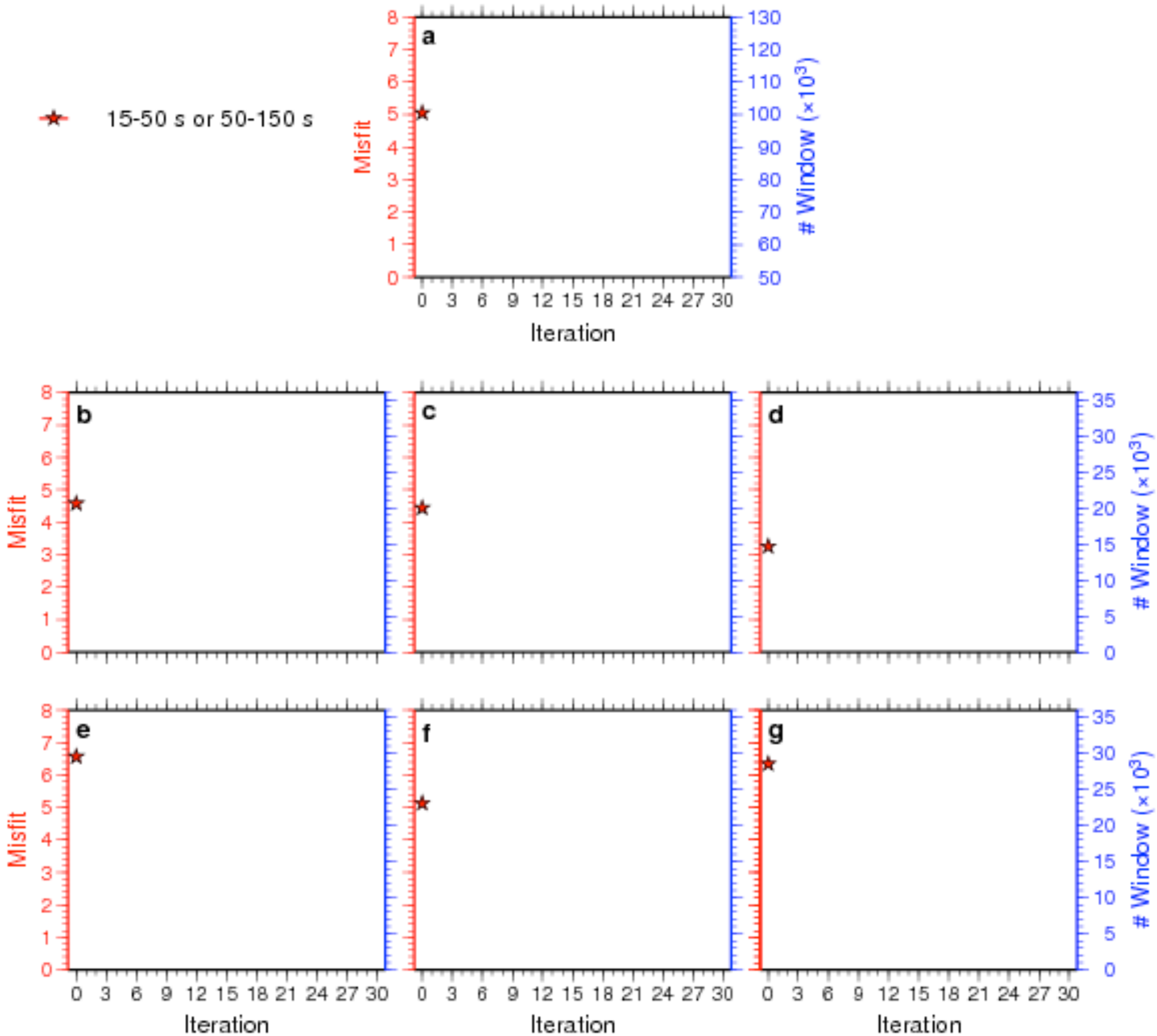
15-50 s or 50-150 s
a
b
c
d
e
f
g
Misfit
Window (×10³)
Iteration

IU.KIEV

DIST: 29.37
BCAZ: 316.05
EVDP: 8.70
EVLO: −21.17
EVLA: 63.93
STLO: 29.22
STLA: 50.70
MB: 6.0

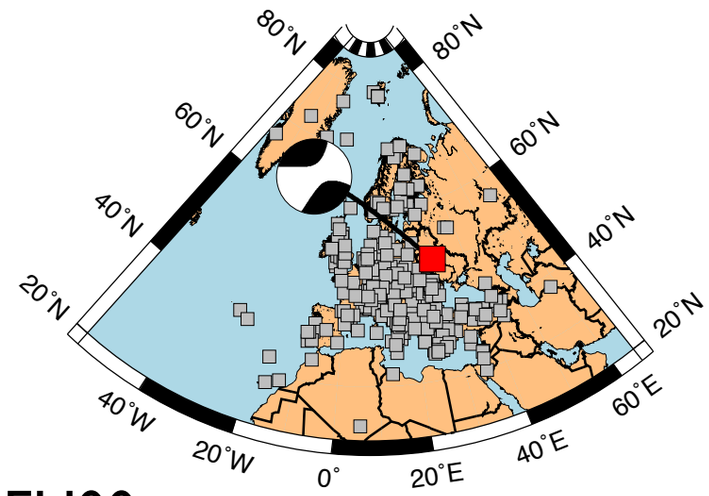

EU00

200805291546A

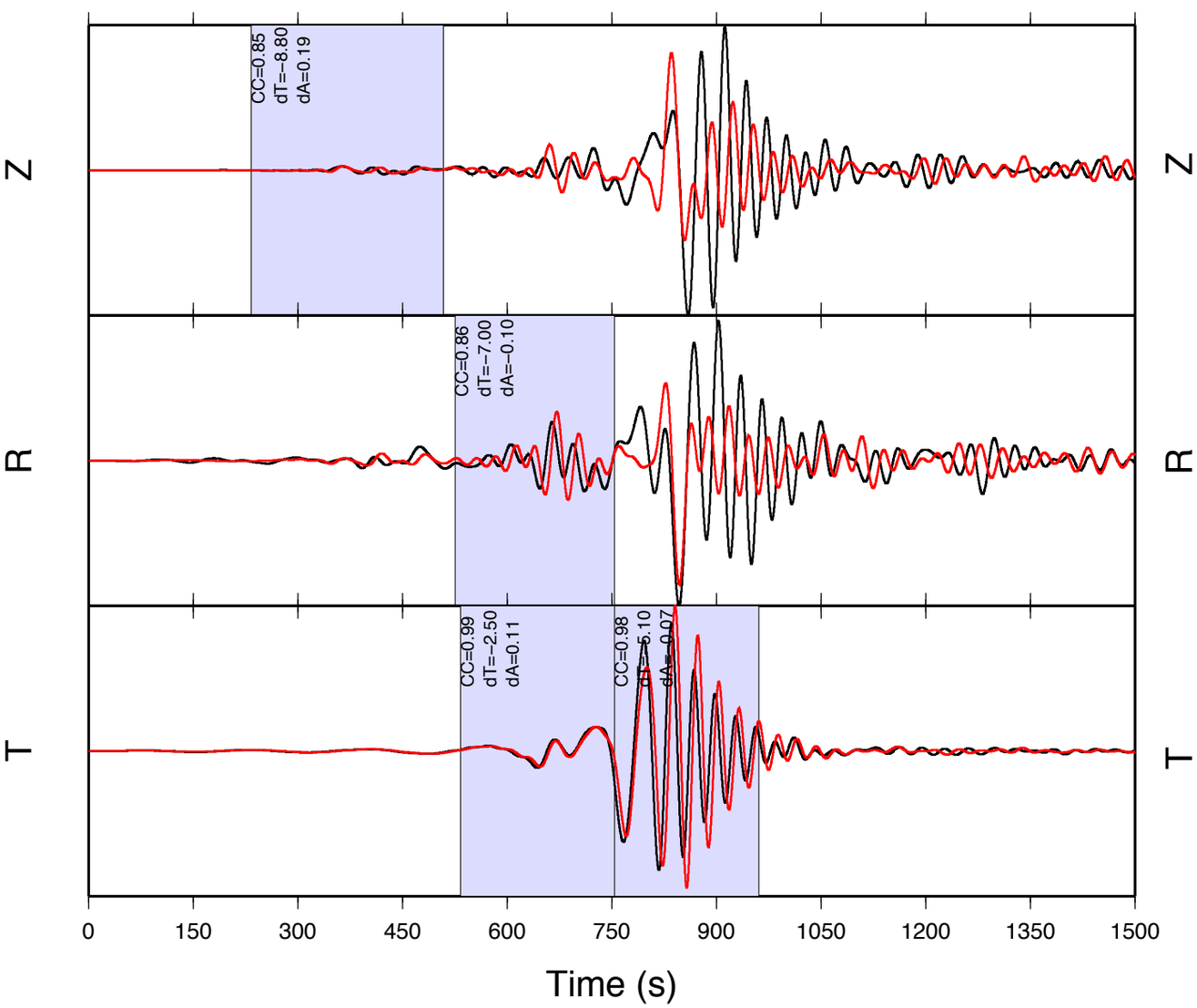

Traveltime Histograms after Elastic Inversion

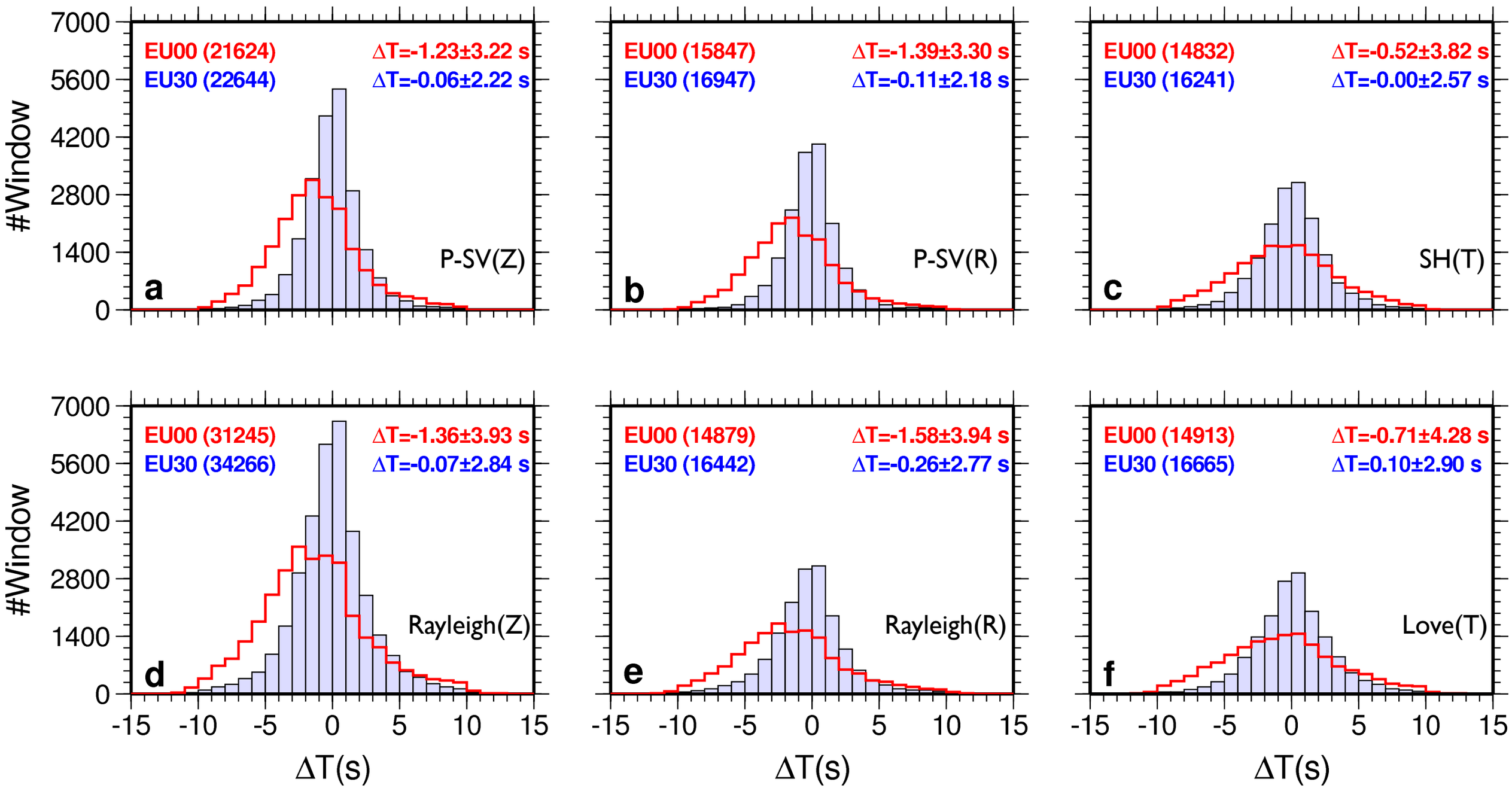

Amplitude Histograms after Elastic Inversion

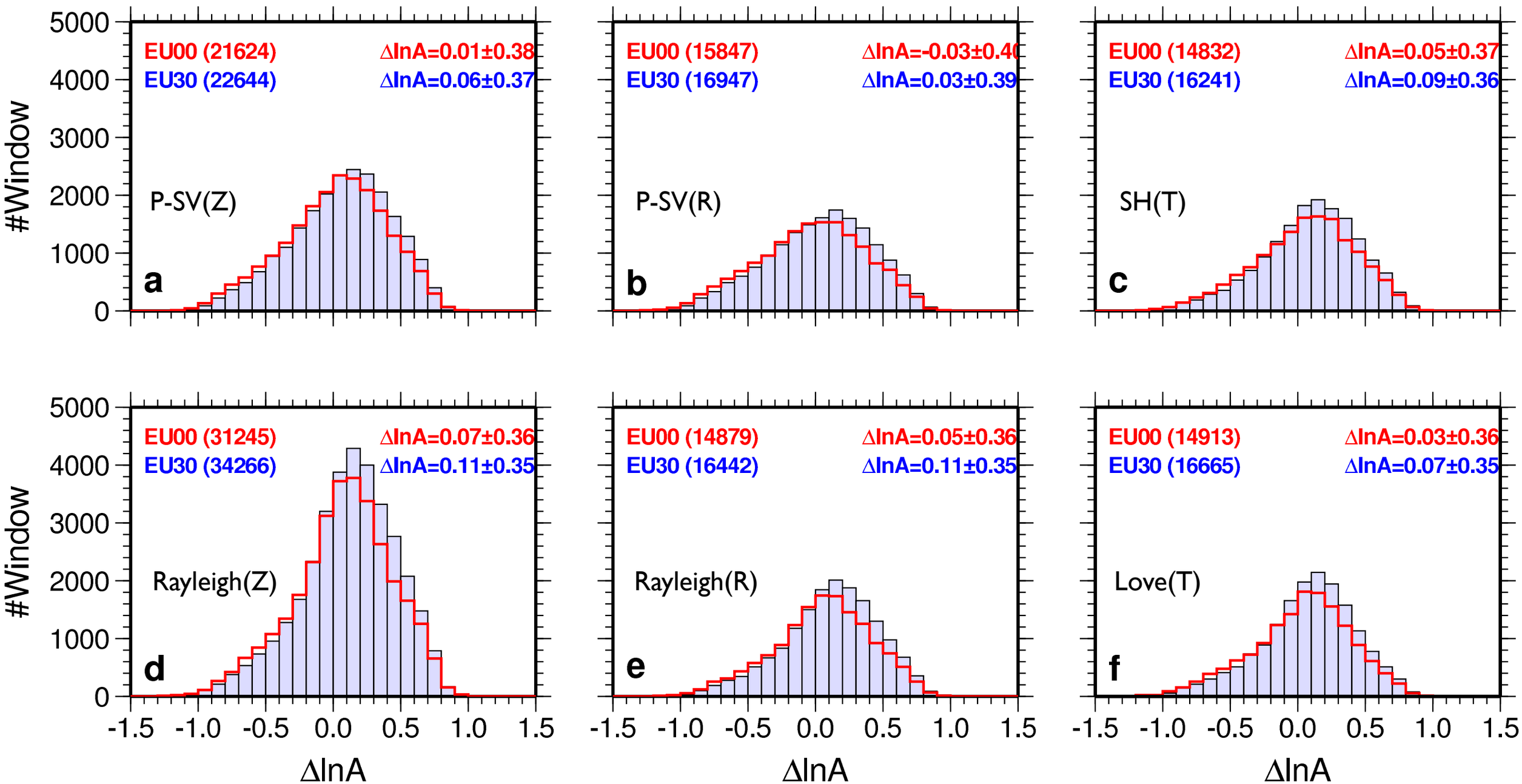

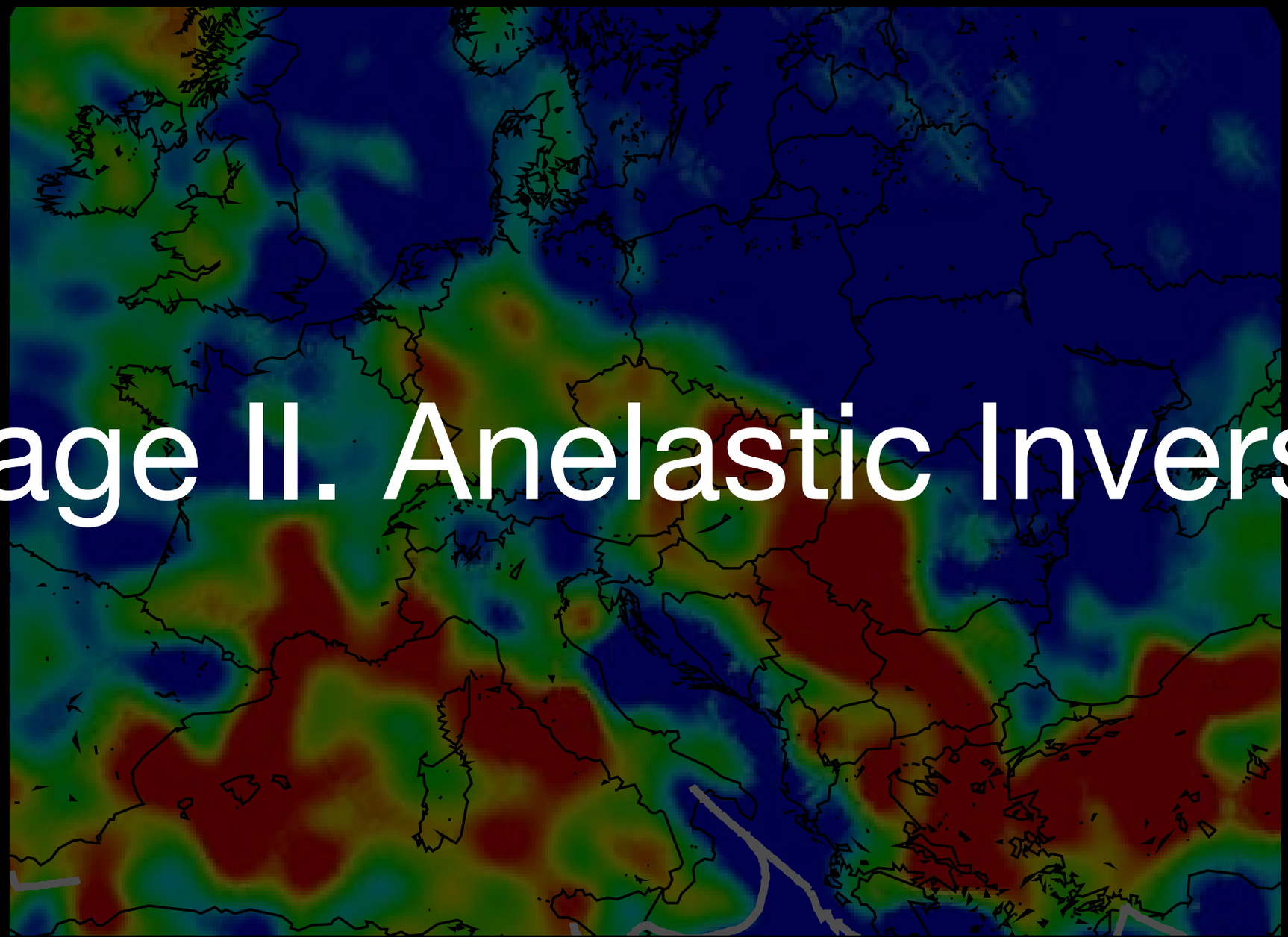

Stage II. Anelastic Inversion

Incorporating Anelasticity in Adjoint Tomography

physical dispersion ↓ amplitude dissipation ↓

$$\mu(\omega) = \mu(\omega_0)[1 + \boxed{(2/\pi)Q_\mu^{-1}\ln(|\omega|/\omega_0)} - \boxed{i\mathrm{sgn}(\omega)Q_\mu^{-1}}]$$

$$\frac{\delta\mu(\omega)}{\mu(\omega_0)} = [(2/\pi)\ln(|\omega|/\omega_0) - i\mathrm{sgn}(\omega)]\delta Q_\mu^{-1}$$

Attenuation gradient: $K_{Q_\mu^{-1}} = -\int_0^T 2\mu(\mathbf{x})\mathbf{D}^\dagger(\mathbf{x}, T-t) : \mathbf{D}(\mathbf{x}, t)\mathrm{d}t$

Anelastic adjoint source ↓ Elastic adjoint source ↓

$$\boxed{\tilde{f}_i^\dagger(\mathbf{x}, t)} = \frac{1}{2\pi}\int_{-\infty}^{+\infty}[(2/\pi)\ln(|\omega|/\omega_0) - i\mathrm{sgn}(\omega)]^* \boxed{f_i^\dagger(\mathbf{x}, \omega)}\exp(i\omega t)\mathrm{d}\omega$$

One extra adjoint simulation is required per source

(Liu *et al*, 1976)

Anelastic Misfit Function

Phase misfit ↓ Amplitude misfit ↓

Total misfit: $$\chi = \boxed{w_\phi \chi^\phi} + \boxed{w_A \chi^A}$$

Phase misfit: $$\boxed{\chi^\phi = \sum_{c=1}^{N_c} w_c \sum_{m=1}^{N_m} \int w_m \left[\frac{\Delta\tau_m(\omega)}{\sigma_m^\phi(\omega)} \right]^2 \mathrm{d}\omega}$$

Amplitude misfit: $$\boxed{\chi^A = \sum_{c=1}^{N_c} w_c \sum_{m=1}^{N_m} \int w_m \left[\frac{\Delta \ln A_m(\omega)}{\sigma_m^A(\omega)} \right]^2 \mathrm{d}\omega}$$

Change in misfit:

Elastic adjoint simulation ↓ Anelastic adjoint simulation ↓

$$\delta\chi = \int_{\mathrm{v}} \boxed{\mathrm{K}_{\beta_\mathrm{v}}\, \delta \ln \beta_\mathrm{v} + \mathrm{K}_{\beta_\mathrm{h}}\, \delta \ln \beta_\mathrm{h} + \mathrm{K}_c\, \delta \ln c + \mathrm{K}_\eta\, \delta \ln \eta} + \boxed{\mathrm{K}_{Q^{-1}}\, \delta Q^{-1}} \mathrm{d}^3\mathbf{x}$$

Amplitude Histograms after Anelastic Inversion

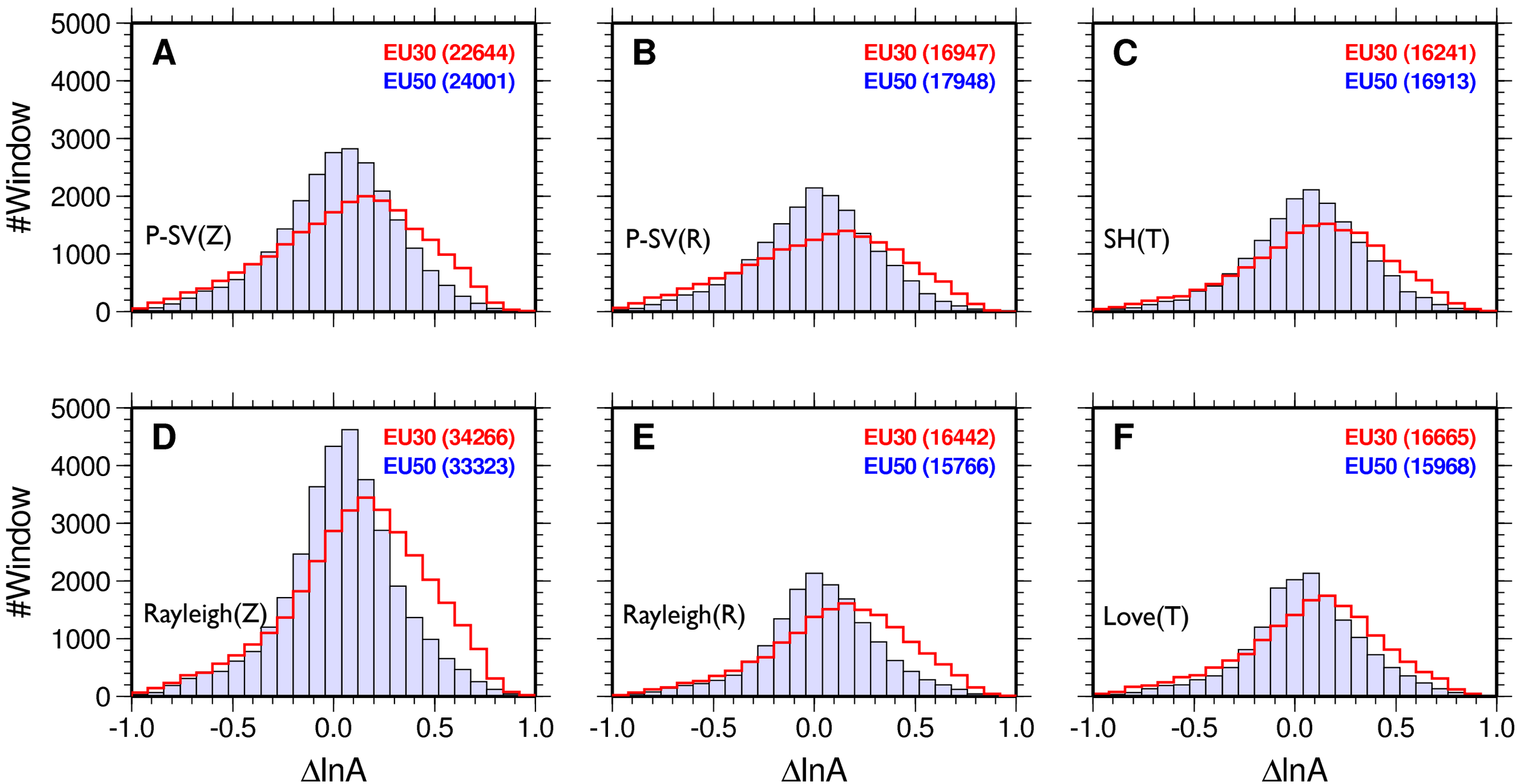

North Atlantic

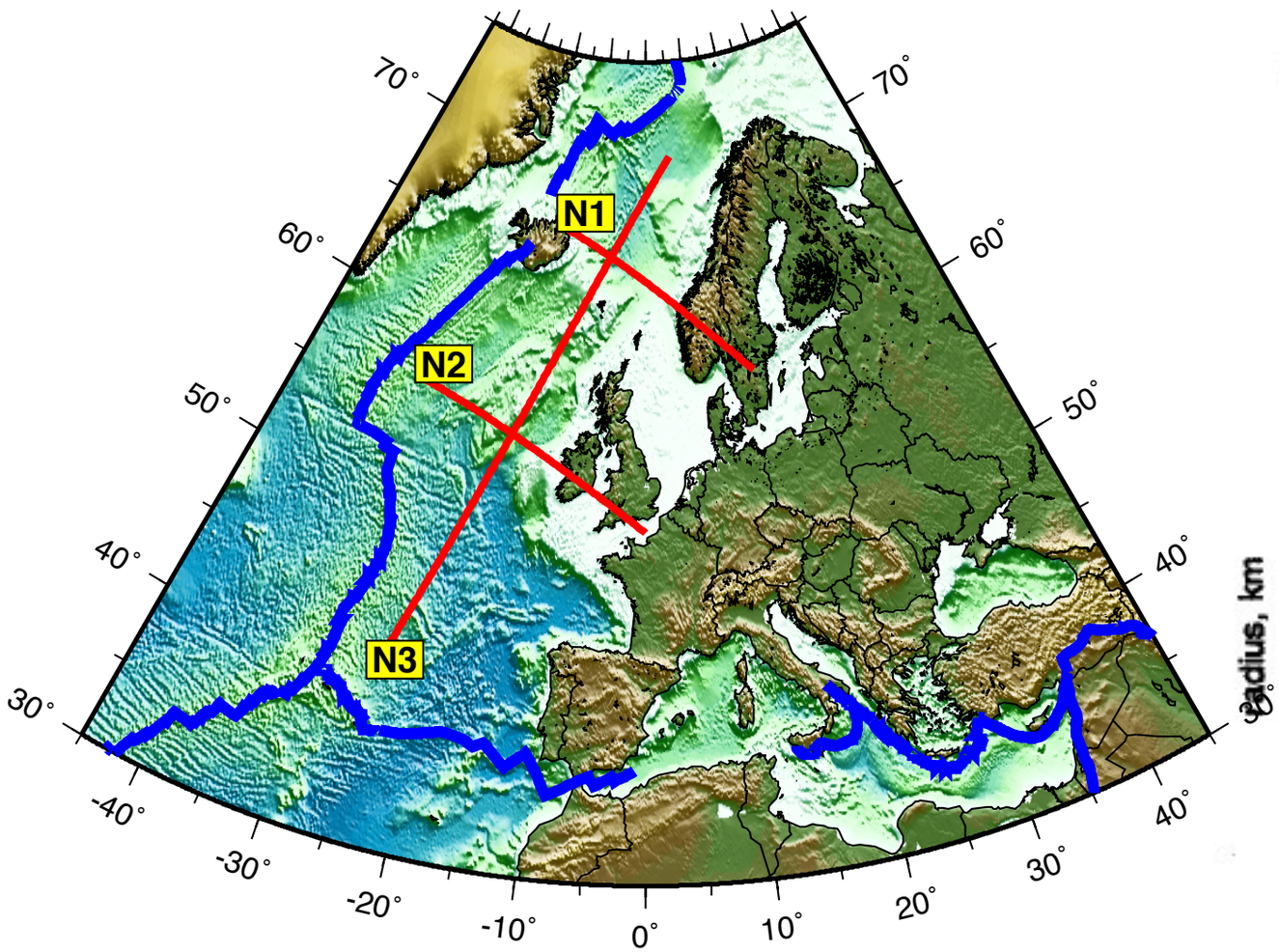

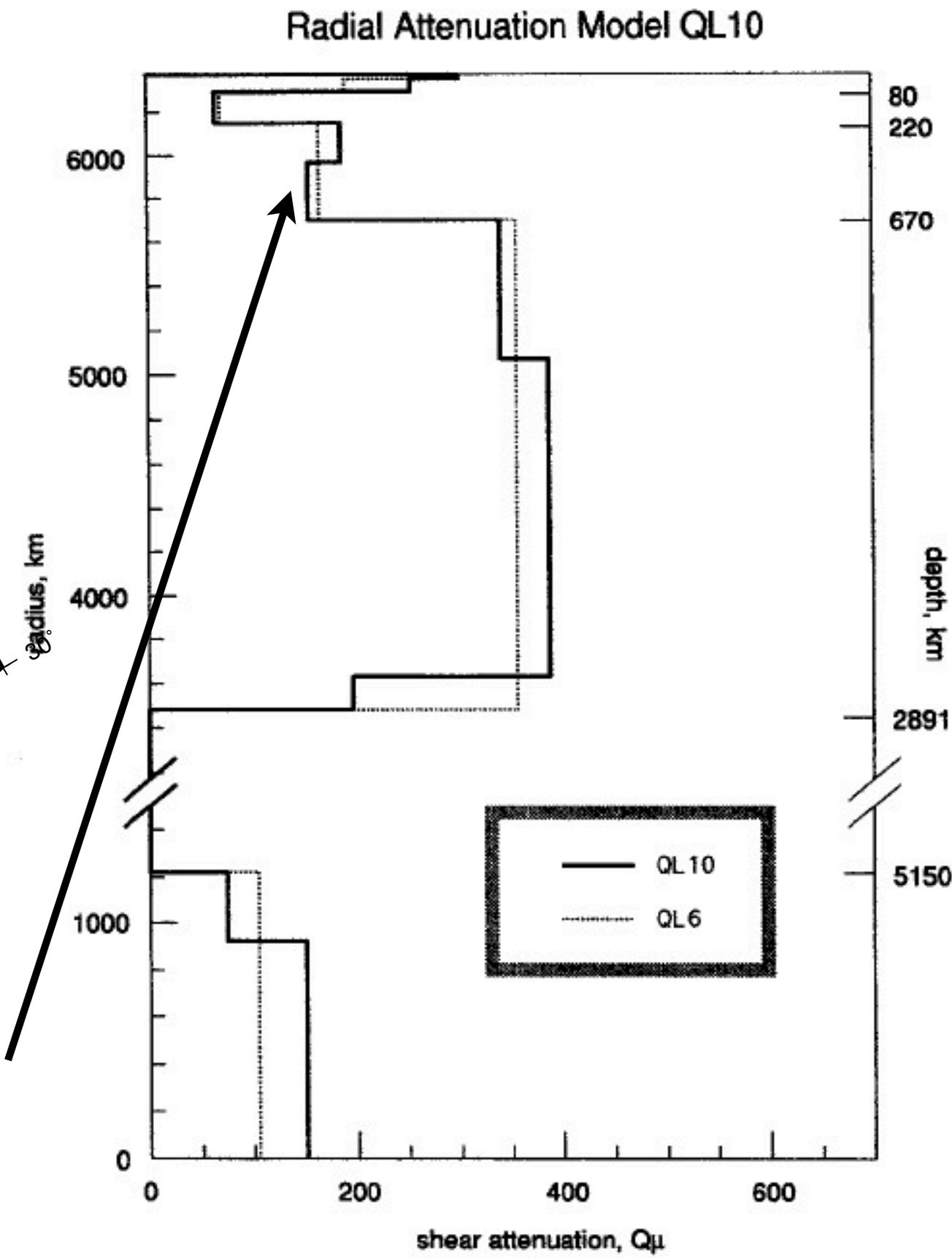

- Oceanic lithosphere (low attenuation)
- Oceanic asthenosphere (high attenuation)
- The lower mantle (reduced attenuation)
- The mantle transition zone (high attenuation)

Implications for Water in the Mantle?

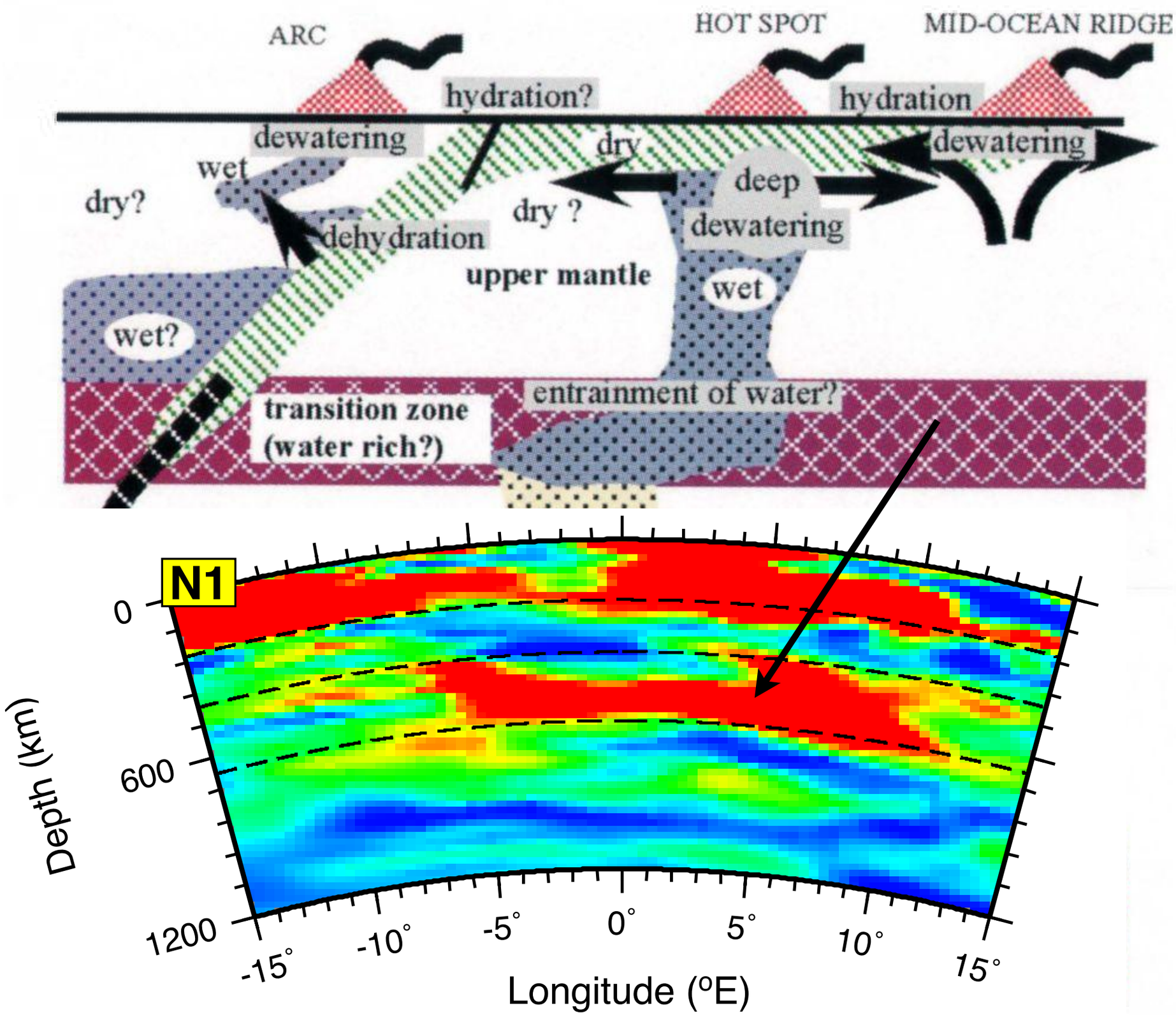

Karato (2006)

Stage III. Anisotropic Inversion

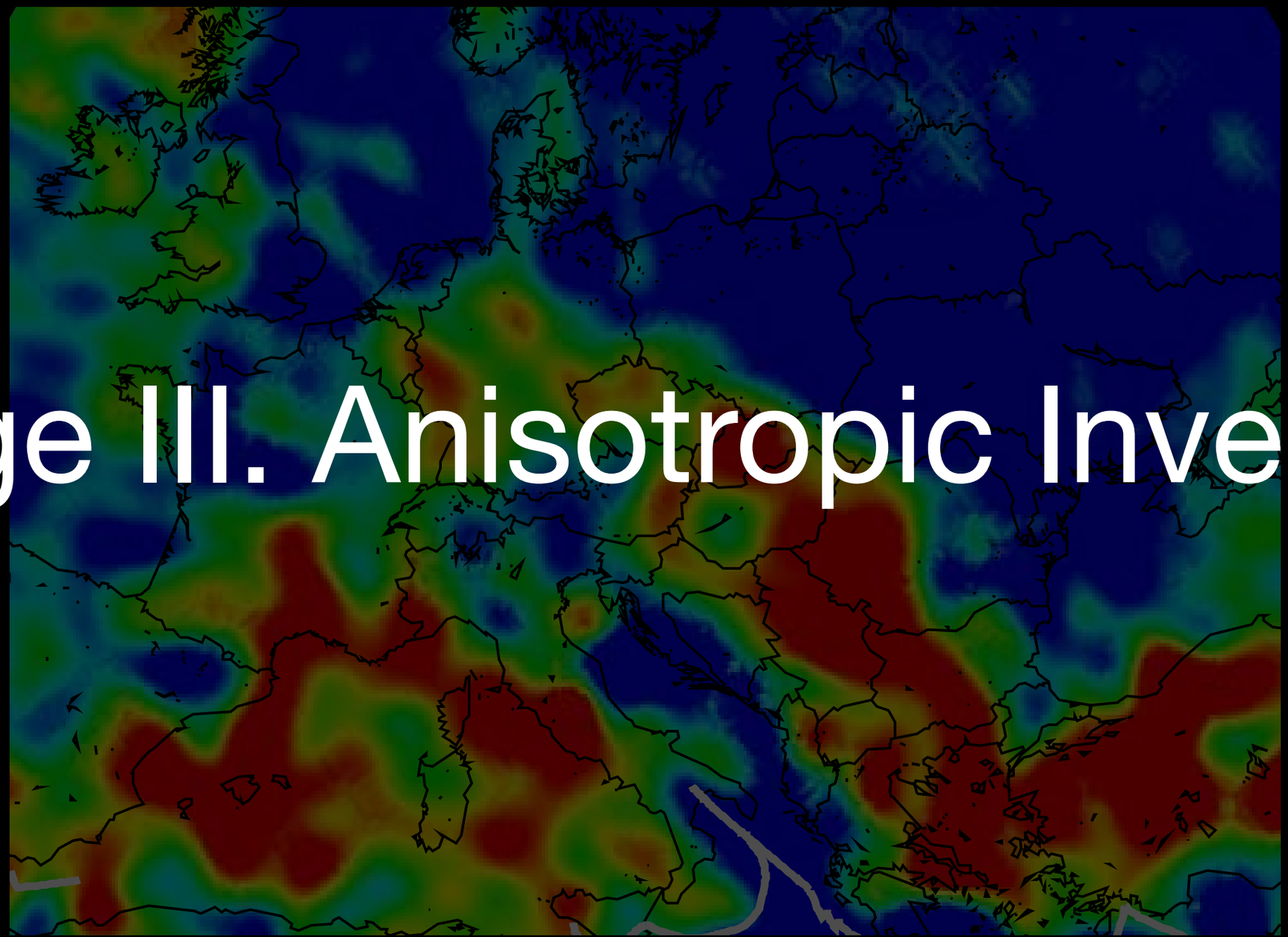

Surface-Wave Anisotropy

Surface-wave phase speed:

$$c(\omega, \theta) = A_0(\omega) + A_1(\omega)\cos(2\theta) + A_2(\omega)\sin(2\theta) + A_3(\omega)\cos(4\theta) + A_4(\omega)\sin(4\theta)$$

Radial anisotropy:

$$A_0(\omega) : A, C, L, N, F$$ (Love, 1927)

Azimuthal anisotropy:

$$A_1(\omega) \text{ and } A_2(\omega) : \boxed{G_c, G_s}, B_c, B_s, H_c, H_s$$

$$A_3(\omega) \text{ and } A_4(\omega) : E_c, E_s$$

(Smith & Dahlen 1973; Montagner & Nataf 1986)

Anisotropic Misfit Function

Phase misfit ↓ Amplitude misfit ↓

Total misfit: $$\chi = \boxed{w_\phi \chi^\phi} + \boxed{w_A \chi^A}$$

Phase misfit: $$\boxed{\chi^\phi = \sum_{c=1}^{N_c} w_c \sum_{m=1}^{N_m} \int w_m \left[\frac{\Delta\tau_m(\omega)}{\sigma_m^\phi(\omega)} \right]^2 \mathrm{d}\omega}$$

Amplitude misfit: $$\boxed{\chi^A = \sum_{c=1}^{N_c} w_c \sum_{m=1}^{N_m} \int w_m \left[\frac{\Delta \ln A_m(\omega)}{\sigma_m^A(\omega)} \right]^2 \mathrm{d}\omega}$$

<u>3 contributions:</u>

- Rayleigh waves (vertical)
- Rayleigh waves (radial)
- Love waves (transverse)

Radial anisotropy ↓ Azimuthal anisotropy ↓

$$\delta\chi = \int_{\mathrm{v}} \boxed{\mathrm{K}_L \delta L + \mathrm{K}_N \delta N} + \boxed{\mathrm{K}_{G_c} \delta G_c + \mathrm{K}_{G_s} \delta G_s} \mathrm{d}^3\mathbf{x}$$

$$\beta_{\mathrm{v}} = \sqrt{L/\rho}$$

$$\beta_{\mathrm{h}} = \sqrt{N/\rho}$$

Anisotropy

Depth 125 km

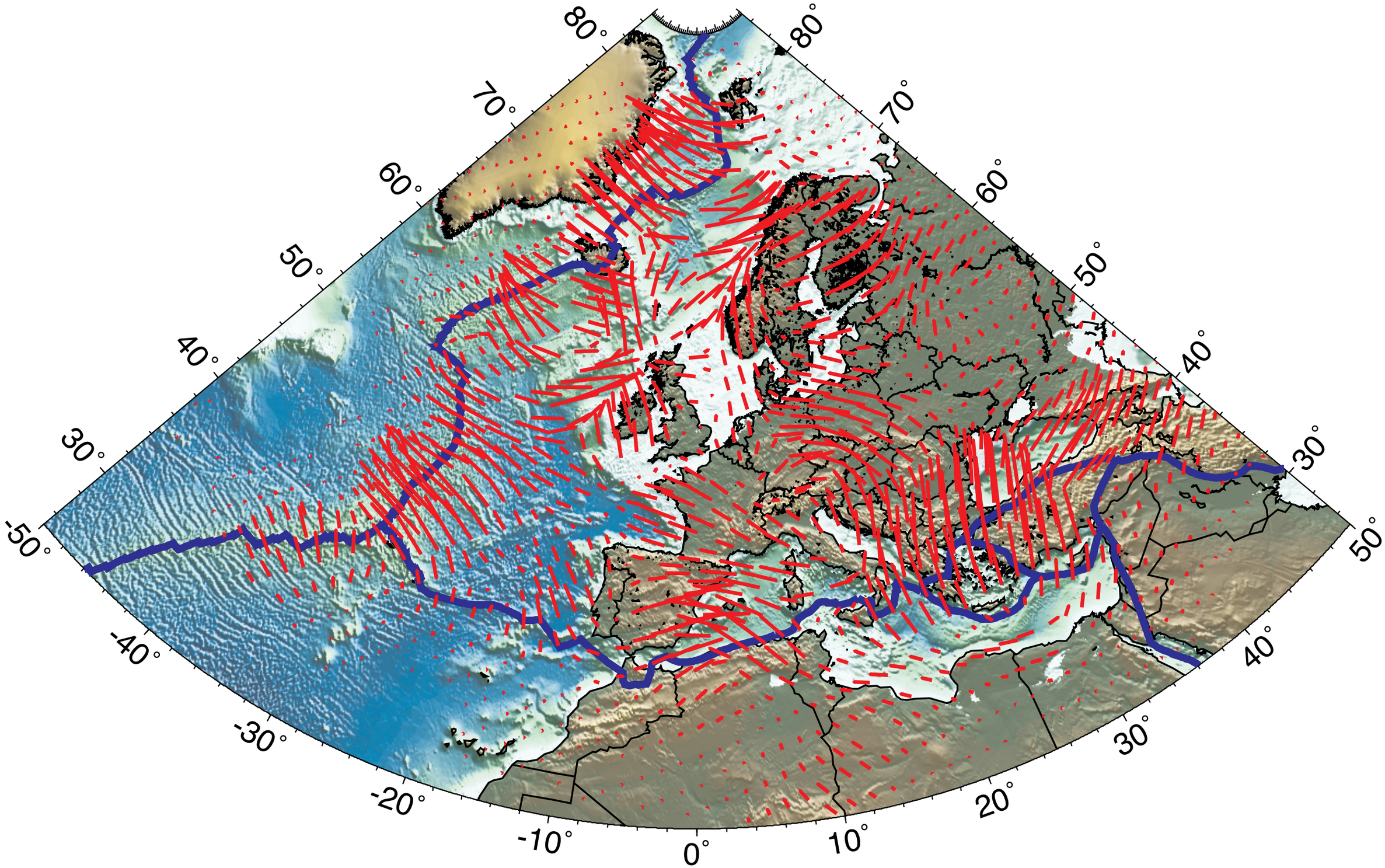

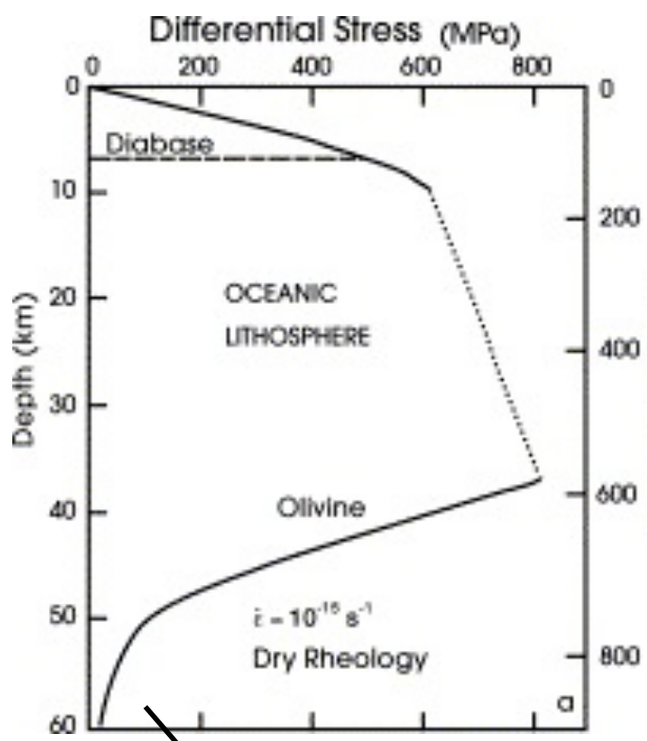
Differential Stress (MPa)
0
200
400
600
800
Diabase
OCEANIC
LITHOSPHERE
Olivine
$\dot{\varepsilon} = 10^{-15}\ s^{-1}$
Dry Rheology
Depth (km)
Temperature (°c)
10
20
30
40
50
60

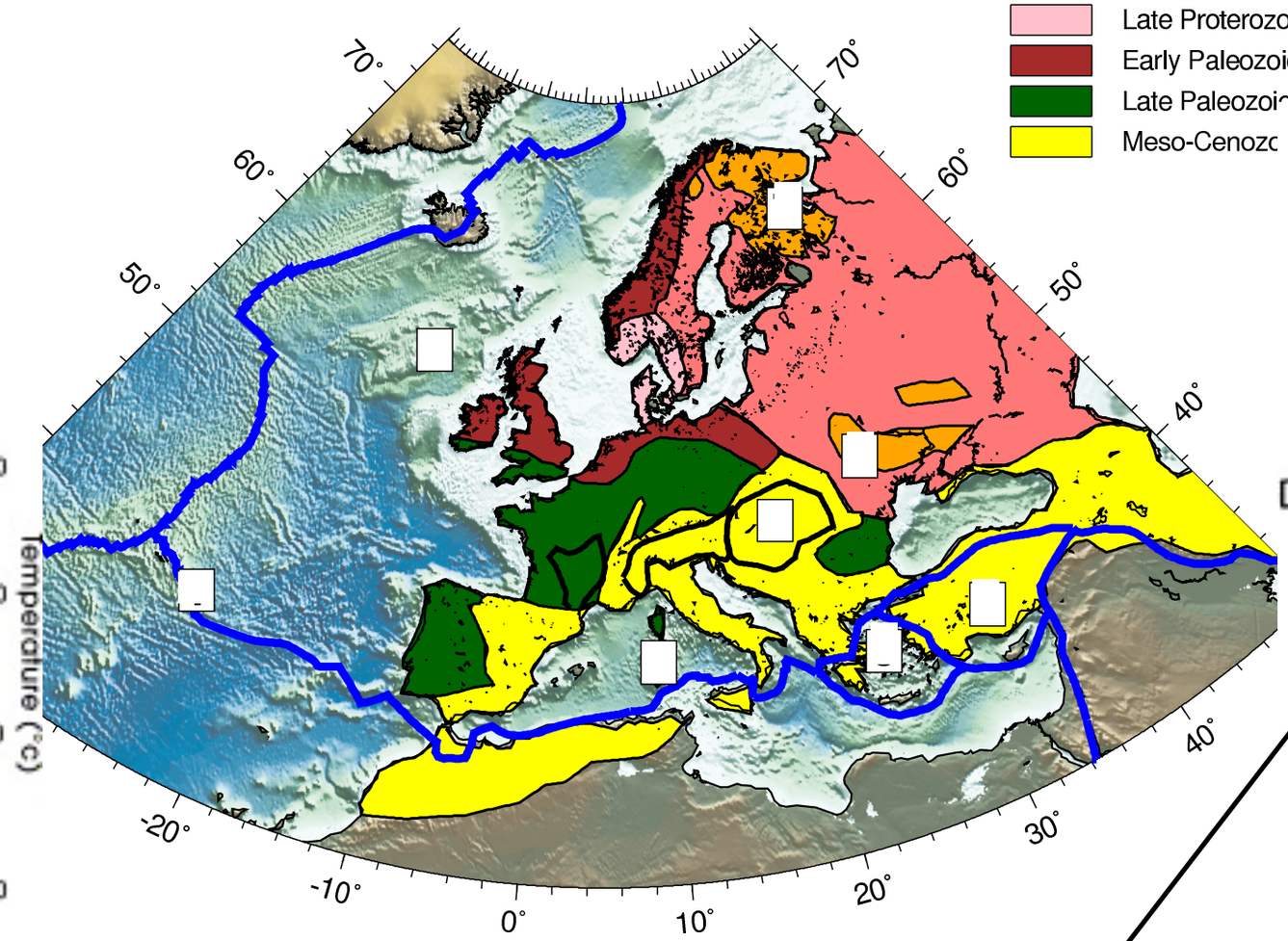
Archaean
Early Proterozoic
Late Proterozoic
Early Paleozoic
Late Paleozoic
Meso-Cenozoic
70°
60°
50°
40°
30°
20°
10°
0°
-10°
-20°

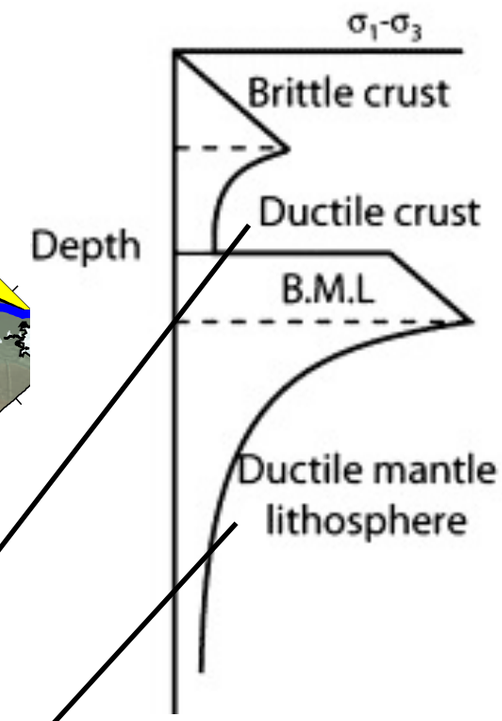
σ_1-σ_3
Brittle crust
Ductile crust
B.M.L
Ductile mantle
lithosphere
Depth

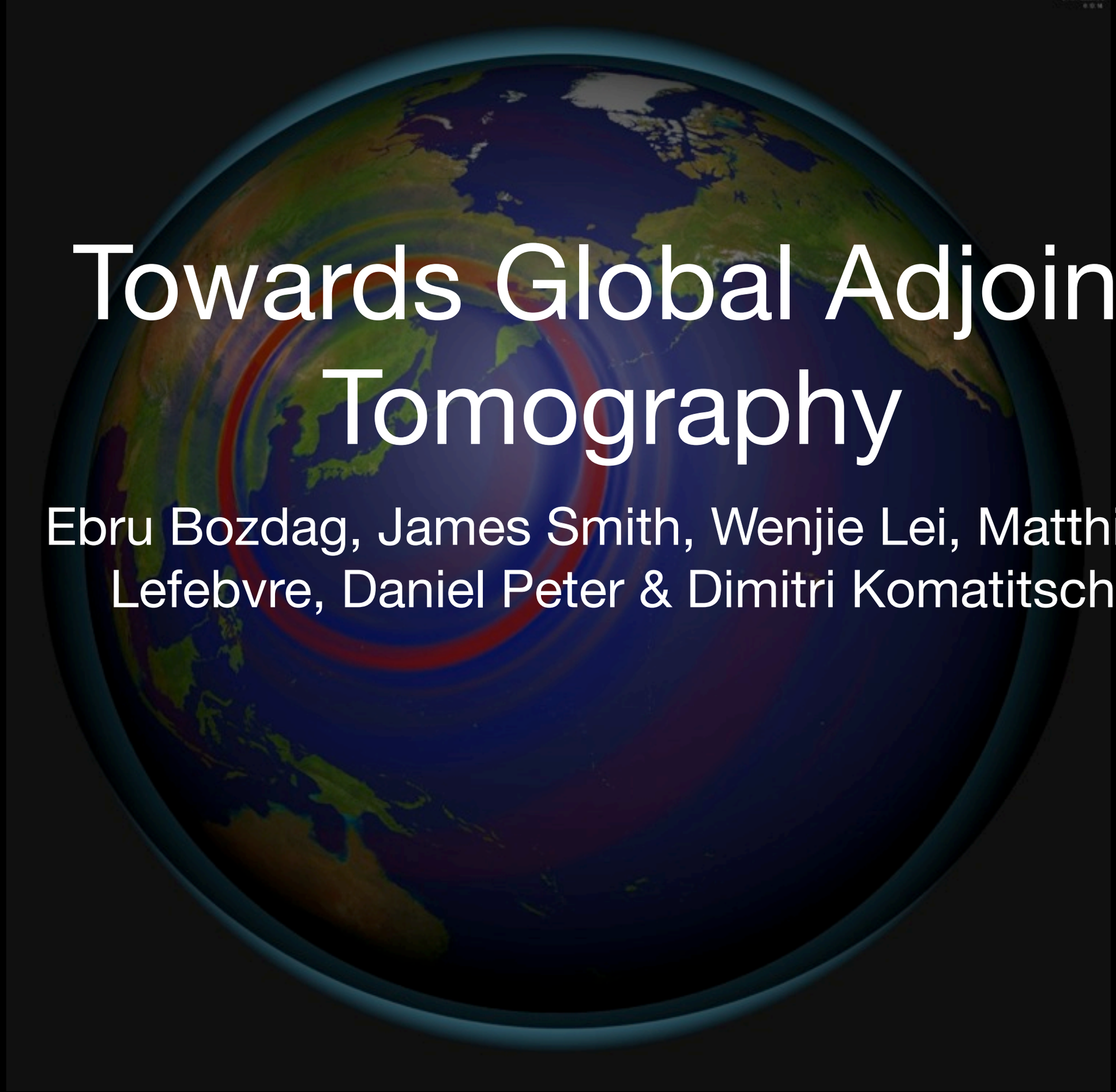

Towards Global Adjoint Tomography

Ebru Bozdag, James Smith, Wenjie Lei, Matthieu Lefebvre, Daniel Peter & Dimitri Komatitsch

Goal on Titan: Use all Global Earthquakes!

~6000 events since 1999 with 5.5 ≤ Mw ≤ 7.0

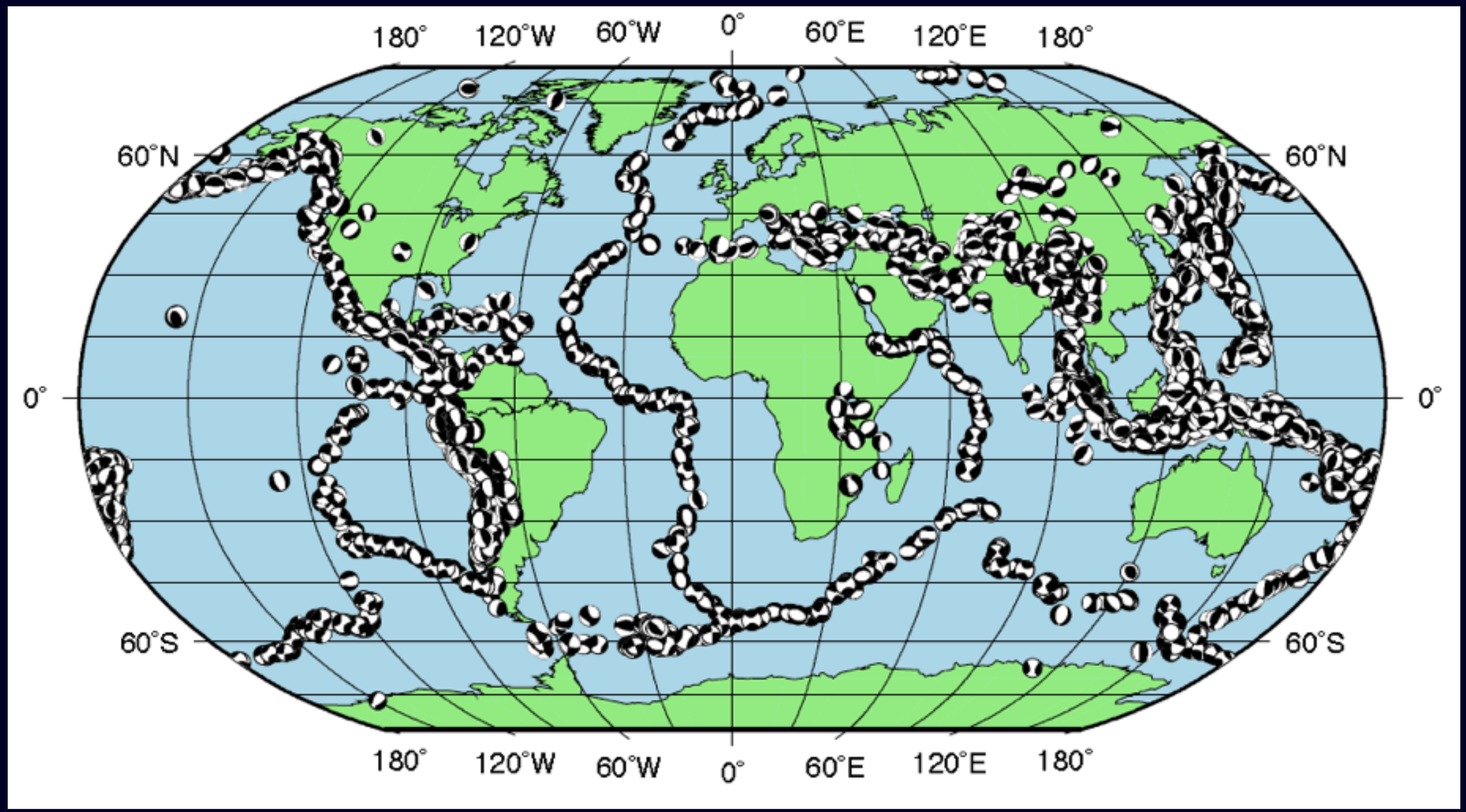

~50 million measurements!

Ebru Bozdag

ORNL Titan: 2013 #2 Supercomputer

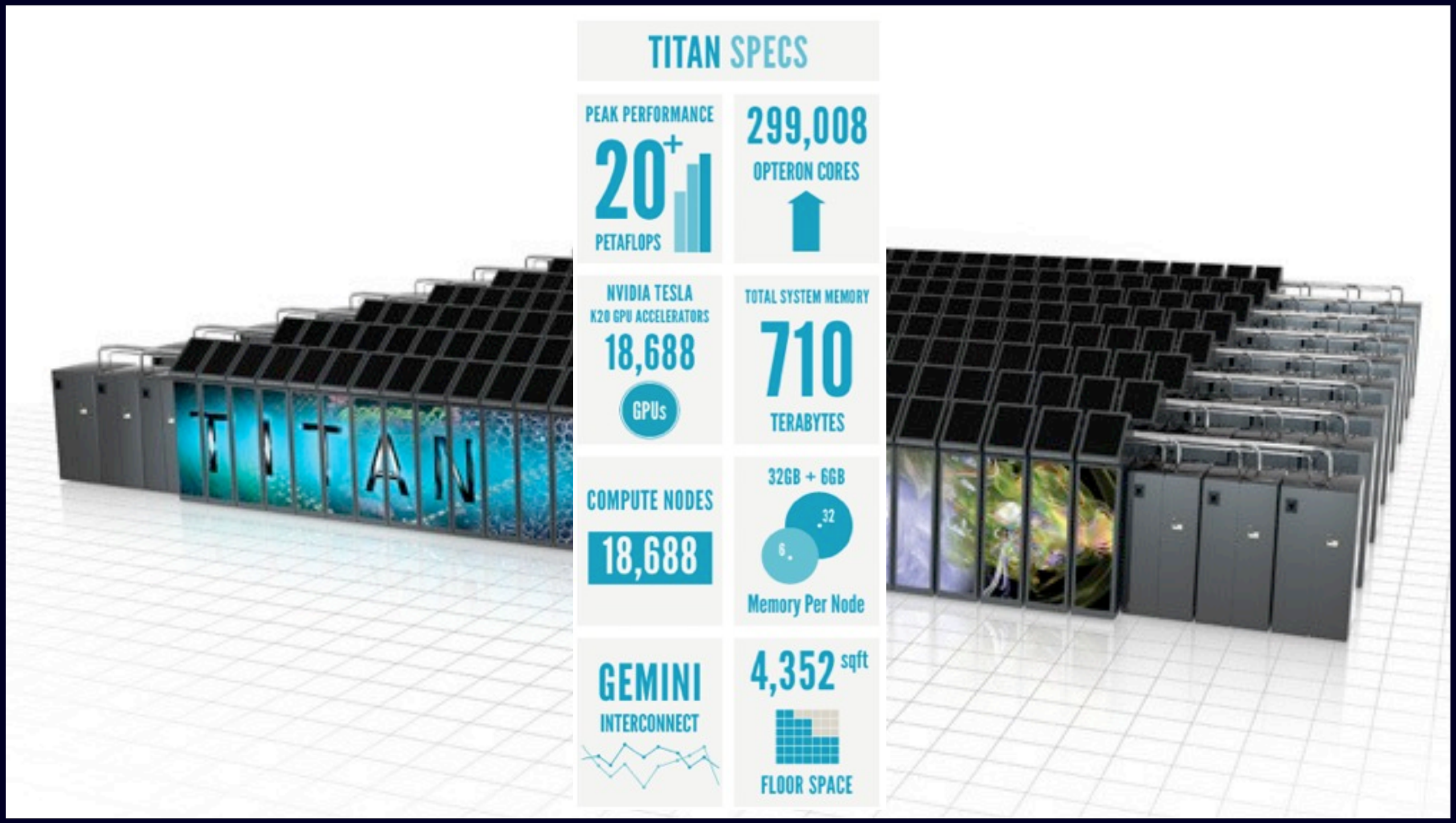

2013 SPECFEM3D_GLOBE allocation: 100M core hours

James Smith Poster
Adaptable Seismic Data Format
(ASDF)

Wenjie Lei Poster
FLEXWIN

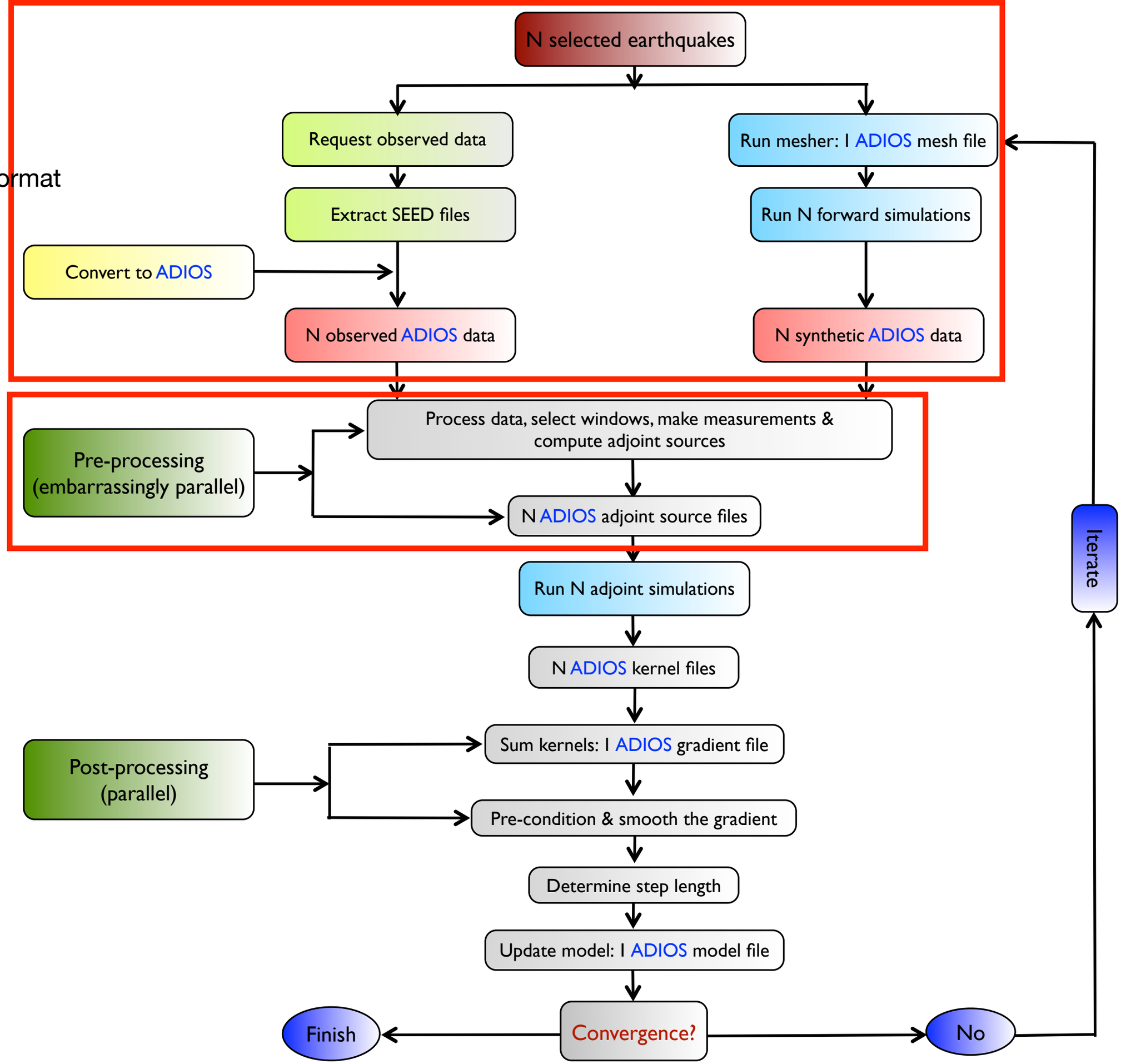

Adaptable Seismic Data Format (ASDF)

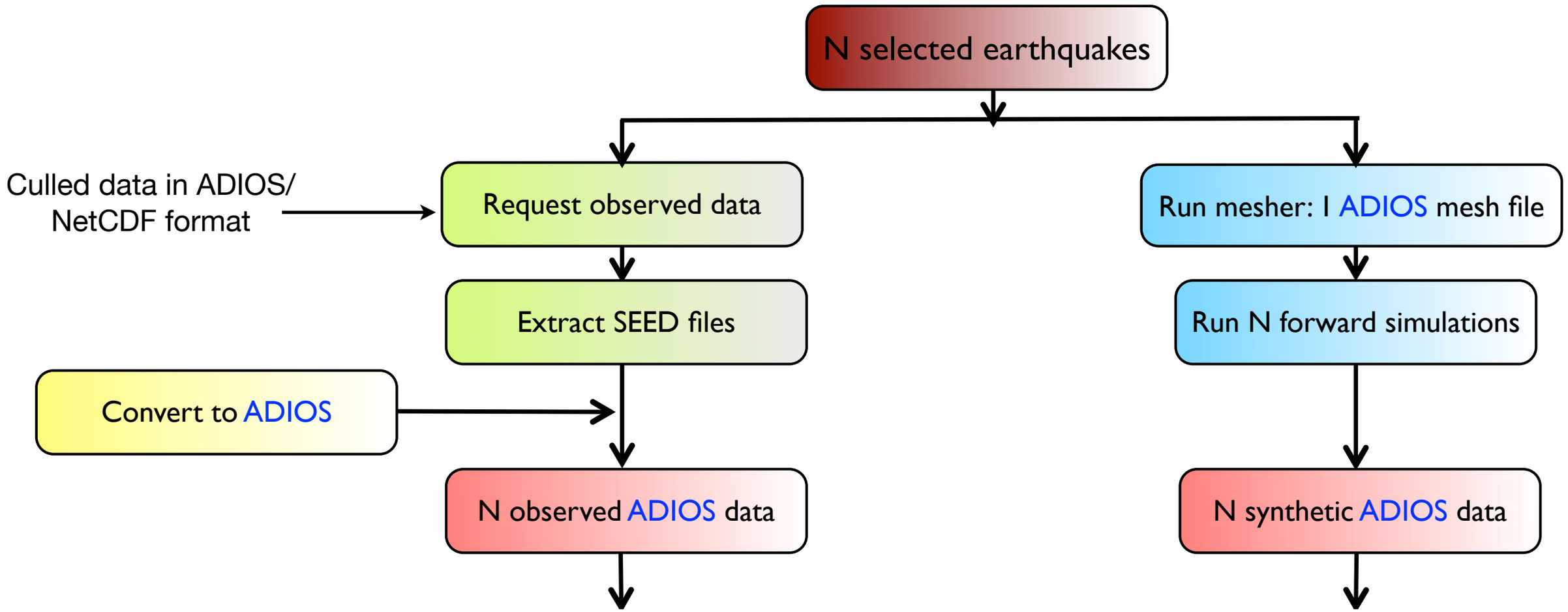

1000 Stations	Number of SAC Files	Number of ADIOS Files
255 Earthquakes	1,275,00	255
6,000 Earthquakes	30,000,000	6,000

Partnerships with Industry, National Labs & HPC Centers

- Petroleum Industry collects, processes and utilizes vast 3D and 4D data sets
- National Labs are developing tools for fast I/O, workflow management, visualization & virtualization
- We should explore potential collaborations focused on:
  - Data formats for fast parallel I/O (e.g., NetCDF, HDF5 & ADIOS)
  - Standard for the exchange of Earth models
  - Cheap, abundant sensors (for, e.g., volcano monitoring, time-lapse migration, dike stability monitoring)
  - Full-waveform imaging and inversion
  - HPC workflow management tools (e.g., Kepler, Pegasus & Swfit)
  - Data mining, feature extraction, visualization & virtualization (e.g., ParaView, Visit)

SHELL GLOBAL
Change Location

Environment & Society

Future of Energy

Meeting demand

Unlocking energy with advanced technologies

Seeing under the surface

Mapping below ground

Robot subs sound out seabed

Seeing clearly beneath the seabed

Seismic: the motion picture

Products & Services

About Shell

Seismic: the motion picture

Shell has found a way to use tiny motion sensors – like those used in modern everyday gadgets – to create sharper pictures of underground rock formations. They could help to find new oil and gas fields more cost effectively.

Geophysicists map underground rock structures by sending seismic waves – essentially sound – through the ground. Sensors record the seismic waves and computers process the recordings to create images of the rock layers. But these seismic images may not be sharp enough to pick up important details. As a result, multi-million dollar exploration wells sometimes end up as dry holes.

The accuracy of seismic imaging could soon improve thanks to a motion sensor, similar to those found in electronic devices like the handheld controllers in a Wii game console. The sensor, developed by computer giant HP and Shell, is 1,000 times more sensitive than those in the Wii.

Dirk Smit, Shell Chief Scientist for Geophysics, was at a nanotechnology conference in late 2008 when he learned of the HP sensor technology. "I realised at once that it could be adapted to record the tiny ground vibrations of exploration seismic waves," he says.

PAGE TOOLS

Conclusions

- The spectral-element method may be used to simulate seismic wave propagation in 3D Earth models
- The adjoint method may be used to calculate misfit gradients with respect to elastic and anelastic model parameters in 3D Earth models
- We are bridging the gap between high-resolution body-wave tomography and lower resolution inversions based on long-period body waves, surface waves and free oscillations
- Frequency-dependent phase and amplitude measurements may be used to simultaneously constrain elastic and anelastic structure
- Simultaneous analysis of wavespeeds, attenuation and anisotropy will improve our understanding of temperature, composition, partial melting and water contents within the Earth's interior

Spot Check Q

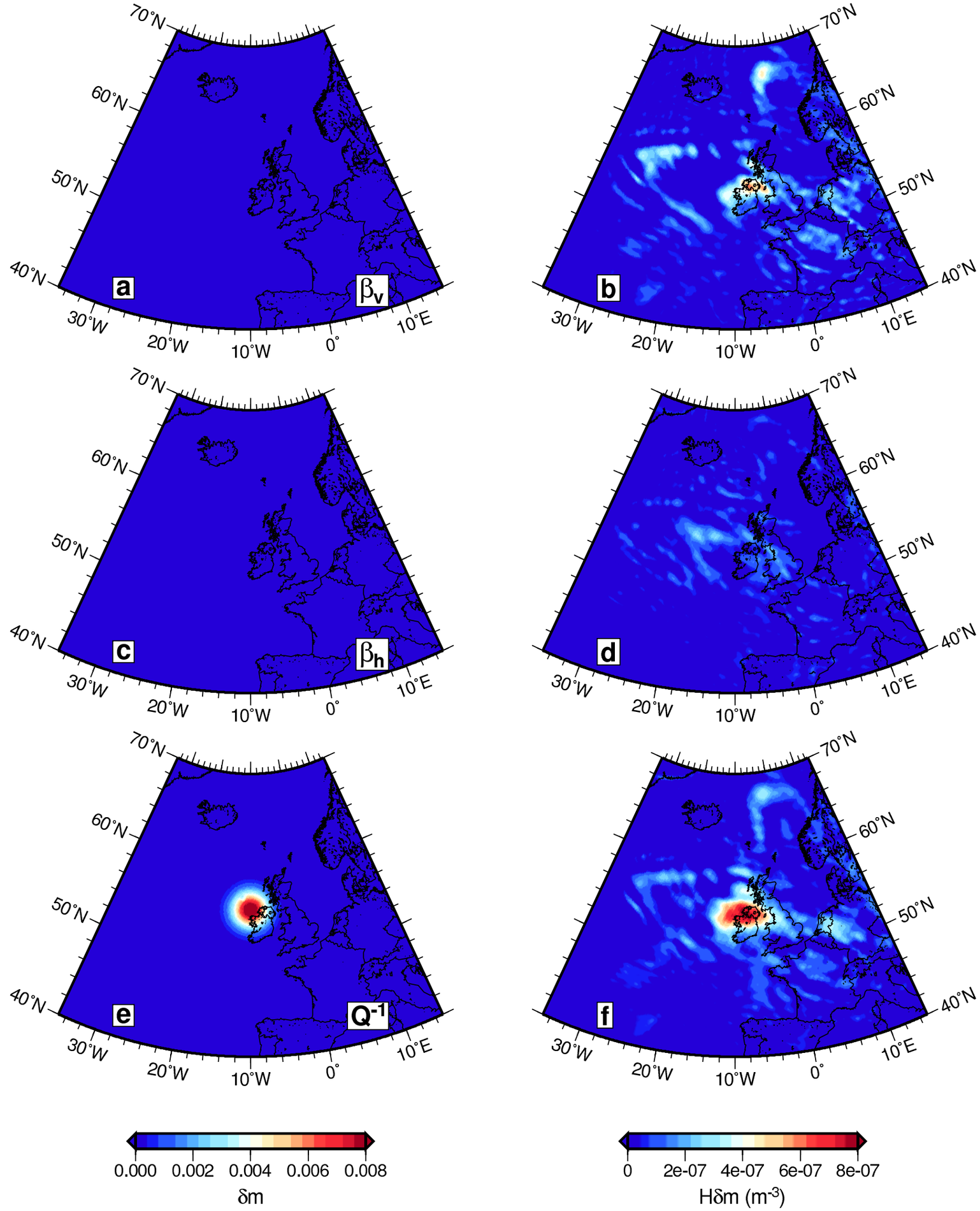
a
β_v
b
c
β_h
d
e
Q^{-1}
f
70°N
60°N
50°N
40°N
30°W
20°W
10°W
0°
10°E
0.000 0.002 0.004 0.006 0.008
δm
0 2e-07 4e-07 6e-07 8e-07
Hδm (m^{-3})

Spot Check Gc

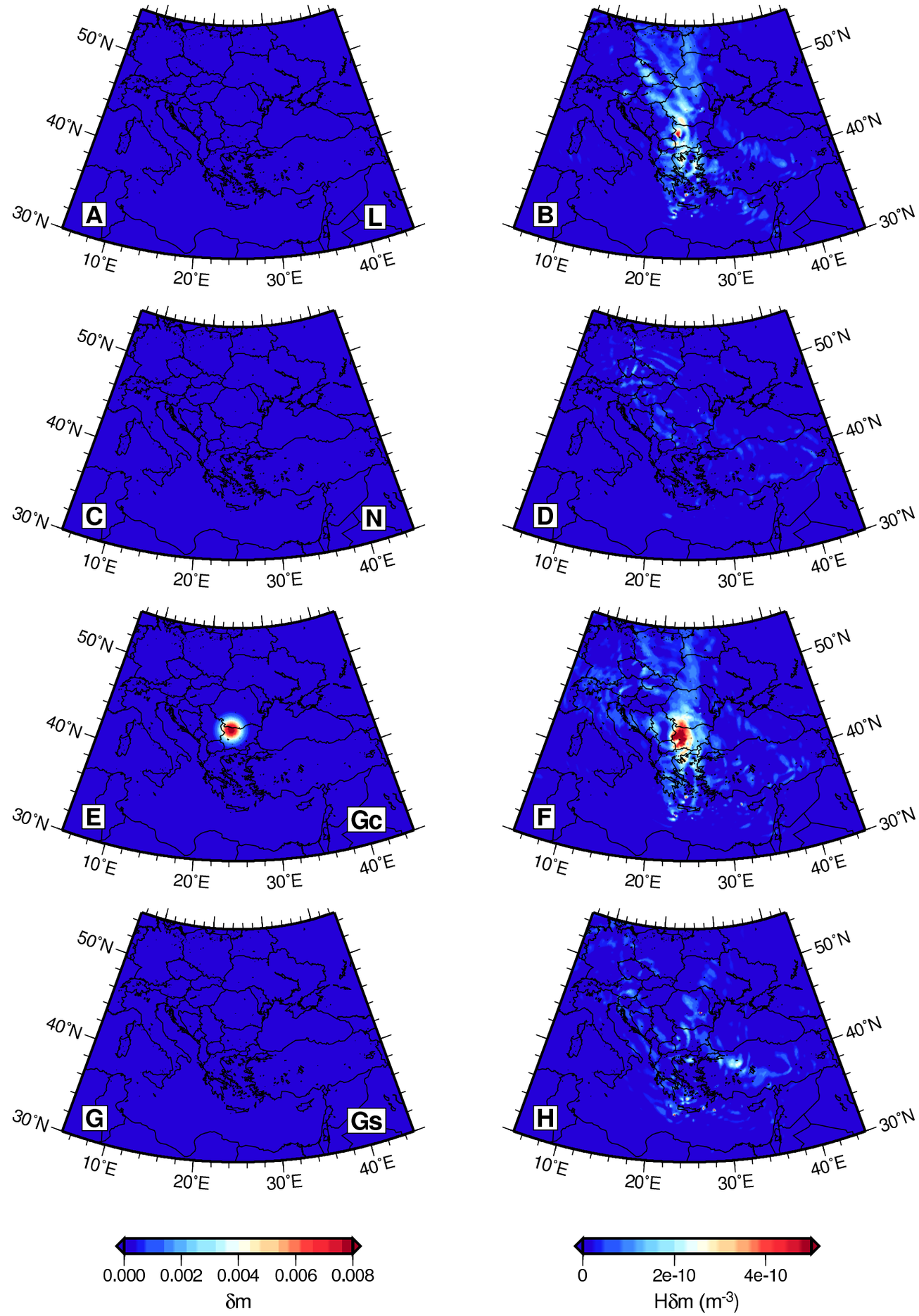

Geological features of EU30 at 75 km

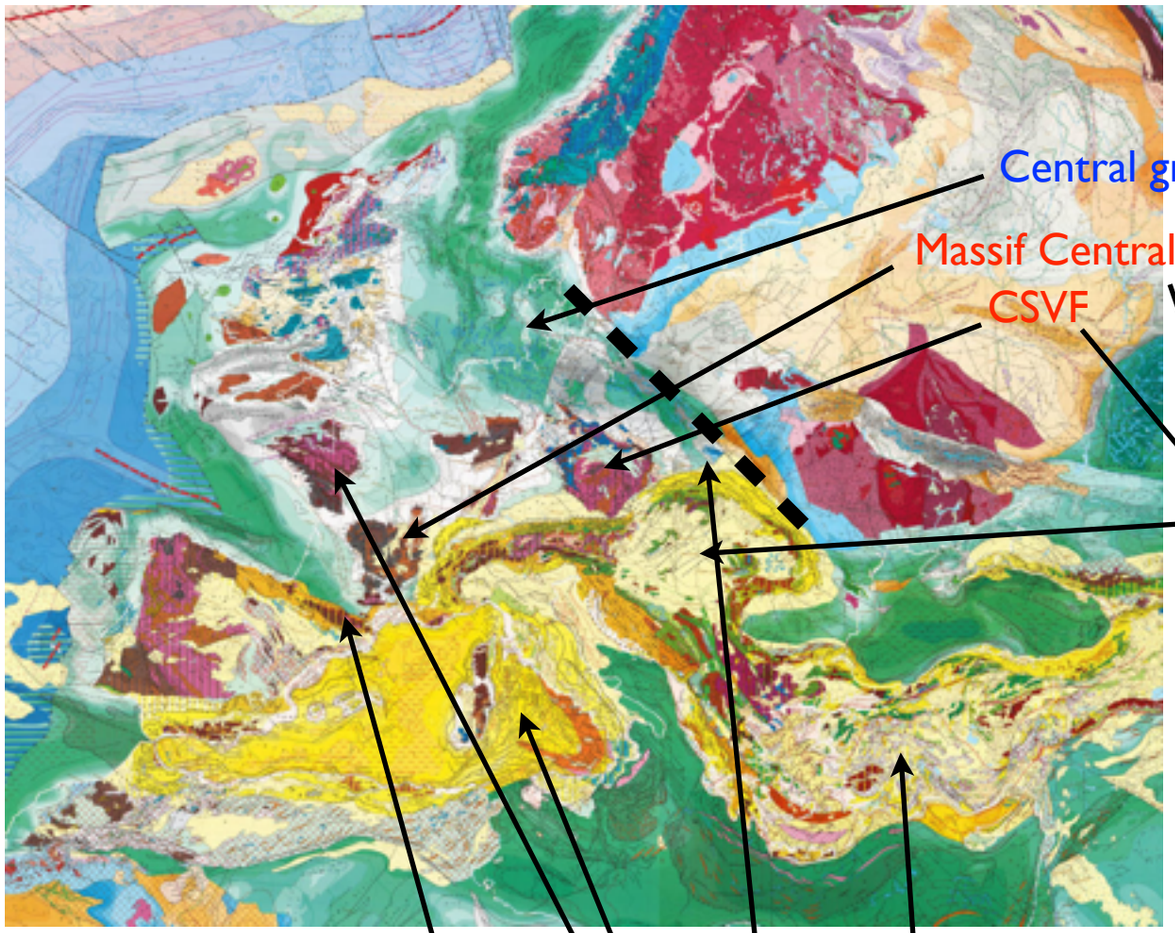

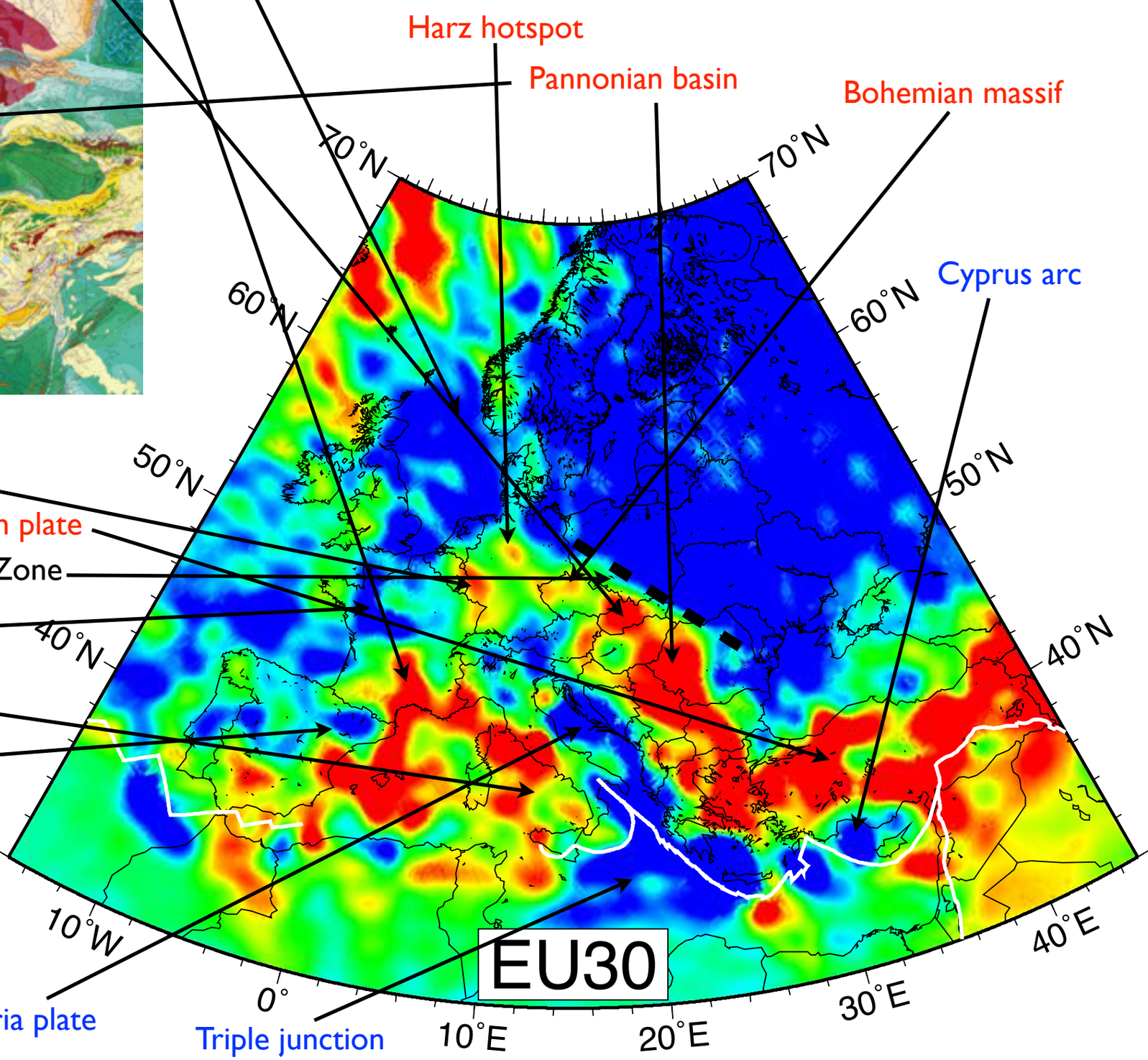

★ CSVF: Central Slovakian Volcanic Field

Comparison of Two Alpine Models

Upper mantle structure beneath the Alpine orogen from high-resolution teleseismic tomography

Regina Lippitsch, Edi Kissling, and Jörg Ansorge
Institute of Geophysics, Swiss Federal Institute of Technology, ETH Hönggerberg, Zürich, Switzerland

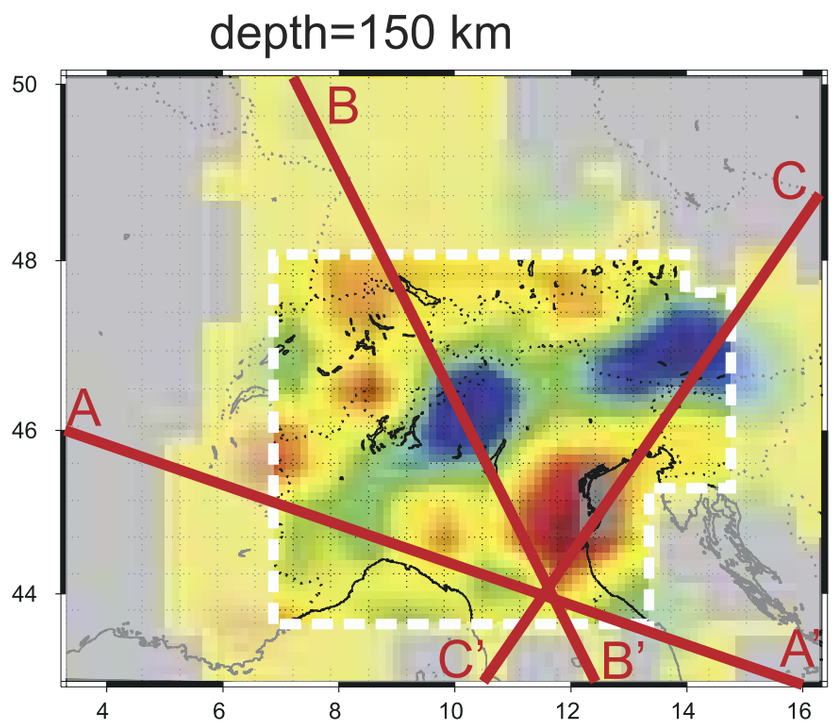

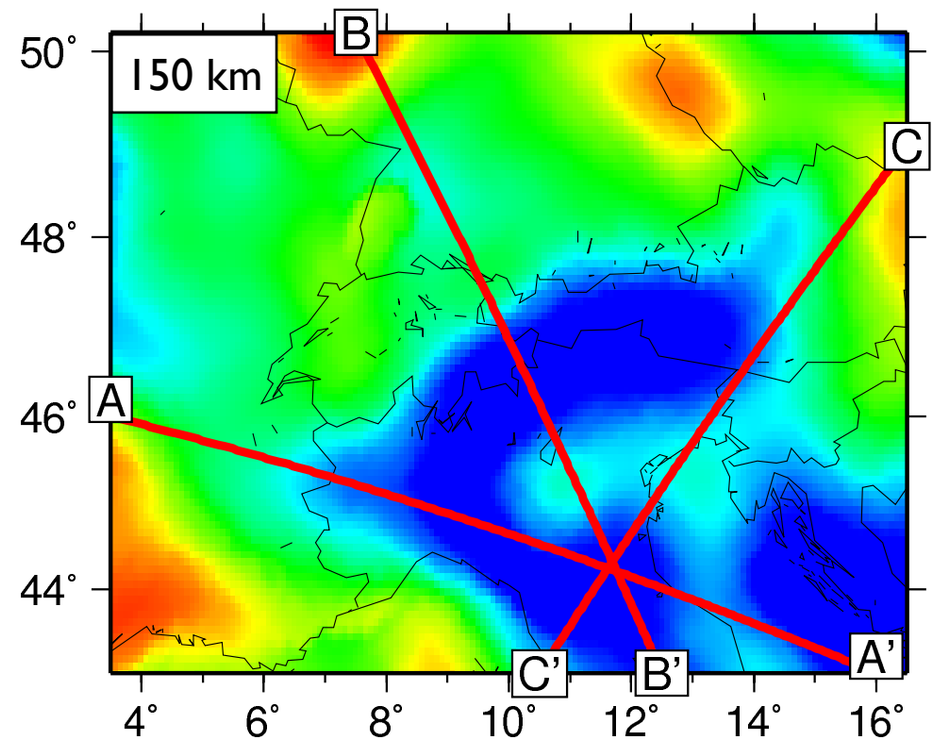

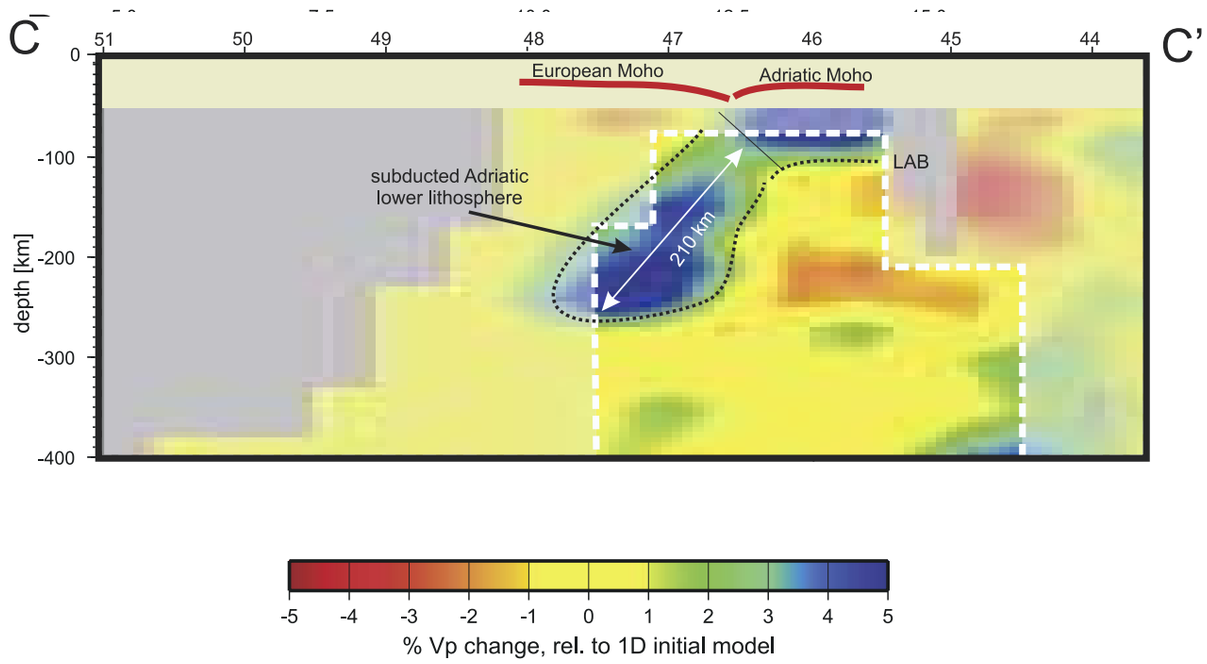

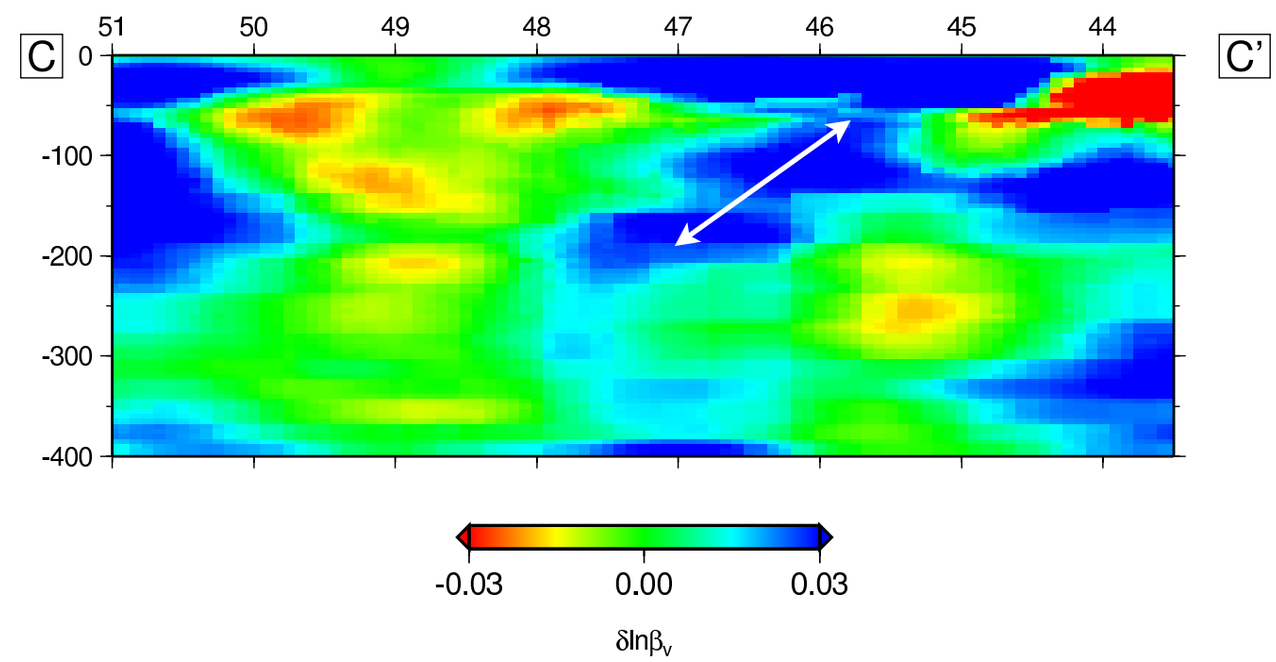

Comparison of Three Transition-Zone Models

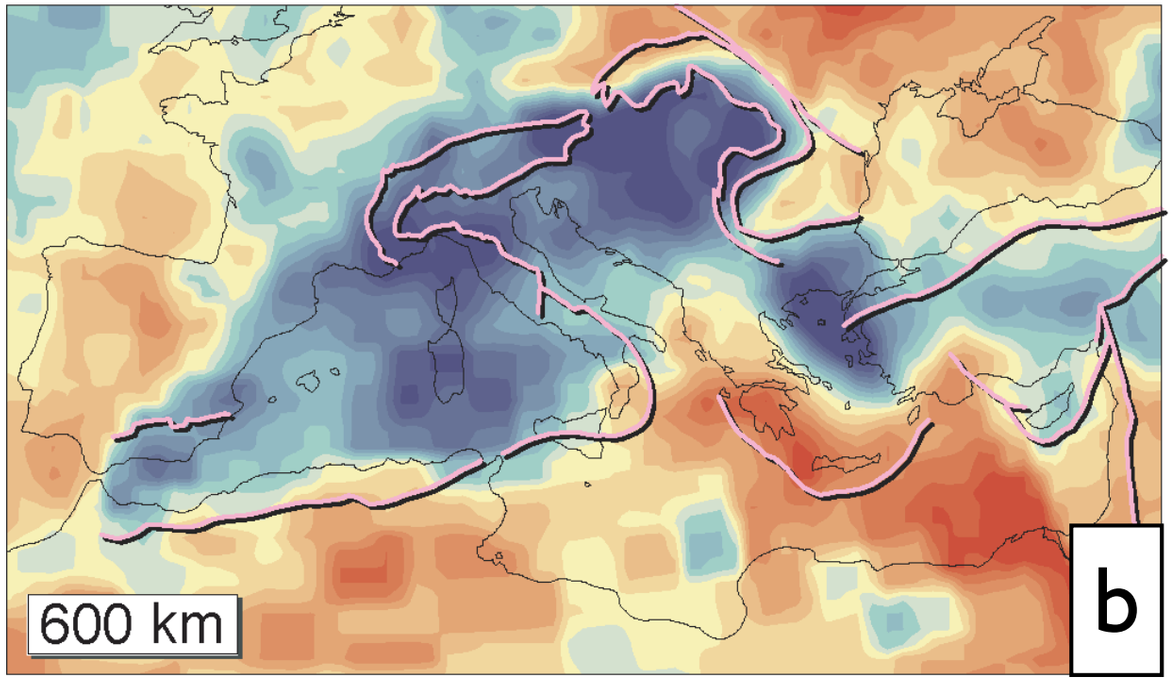

(Wortel & Spakman 2000)

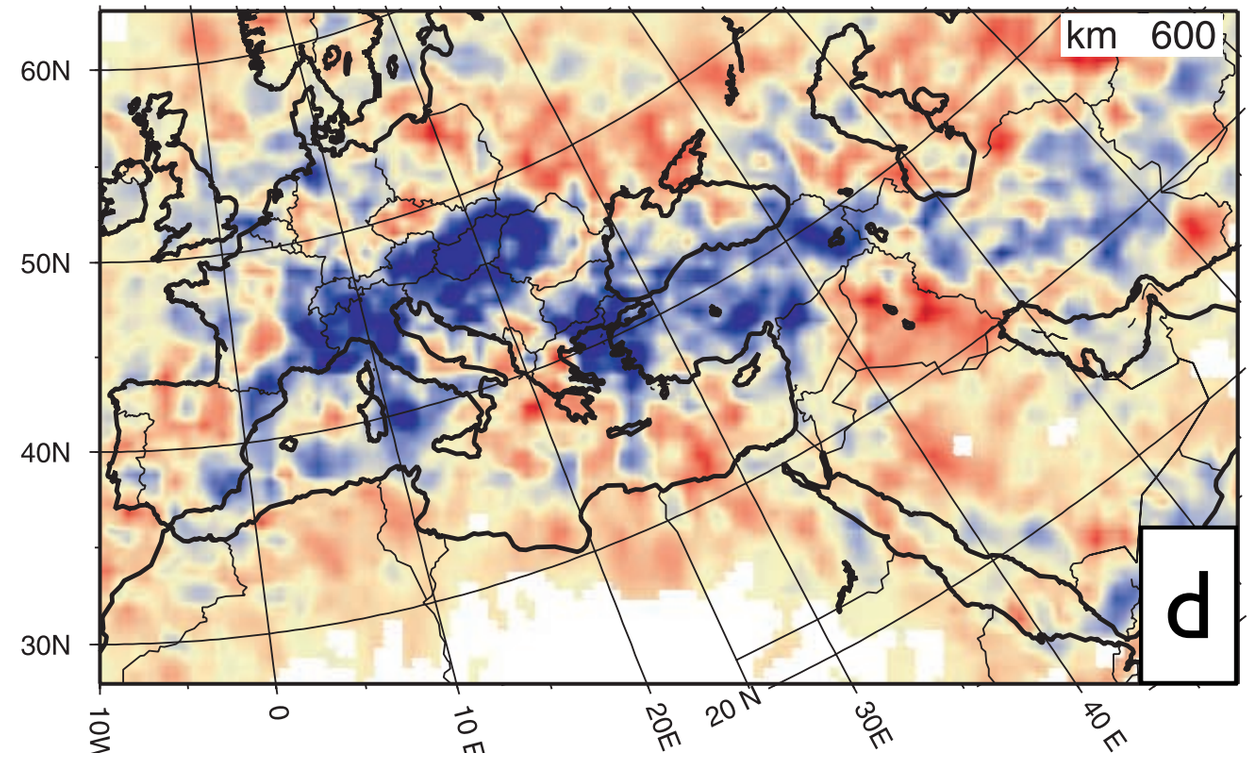

(Piromallo & Morelli 2003)

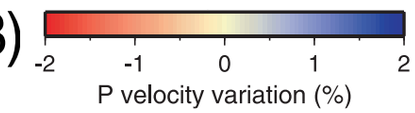

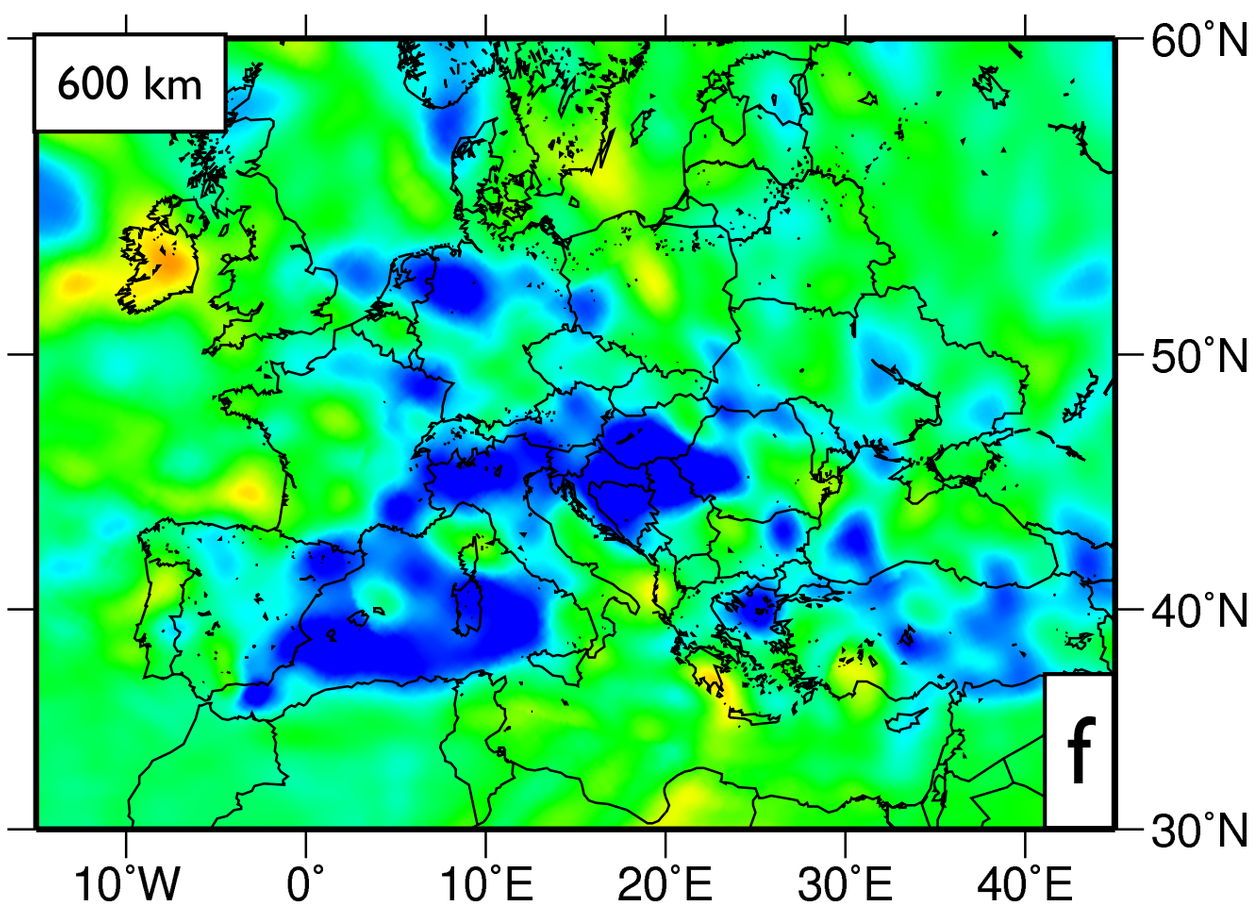

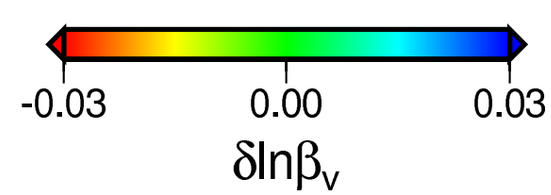

Calabria Slab Model Comparison

(Wortel & Spakman 2000)

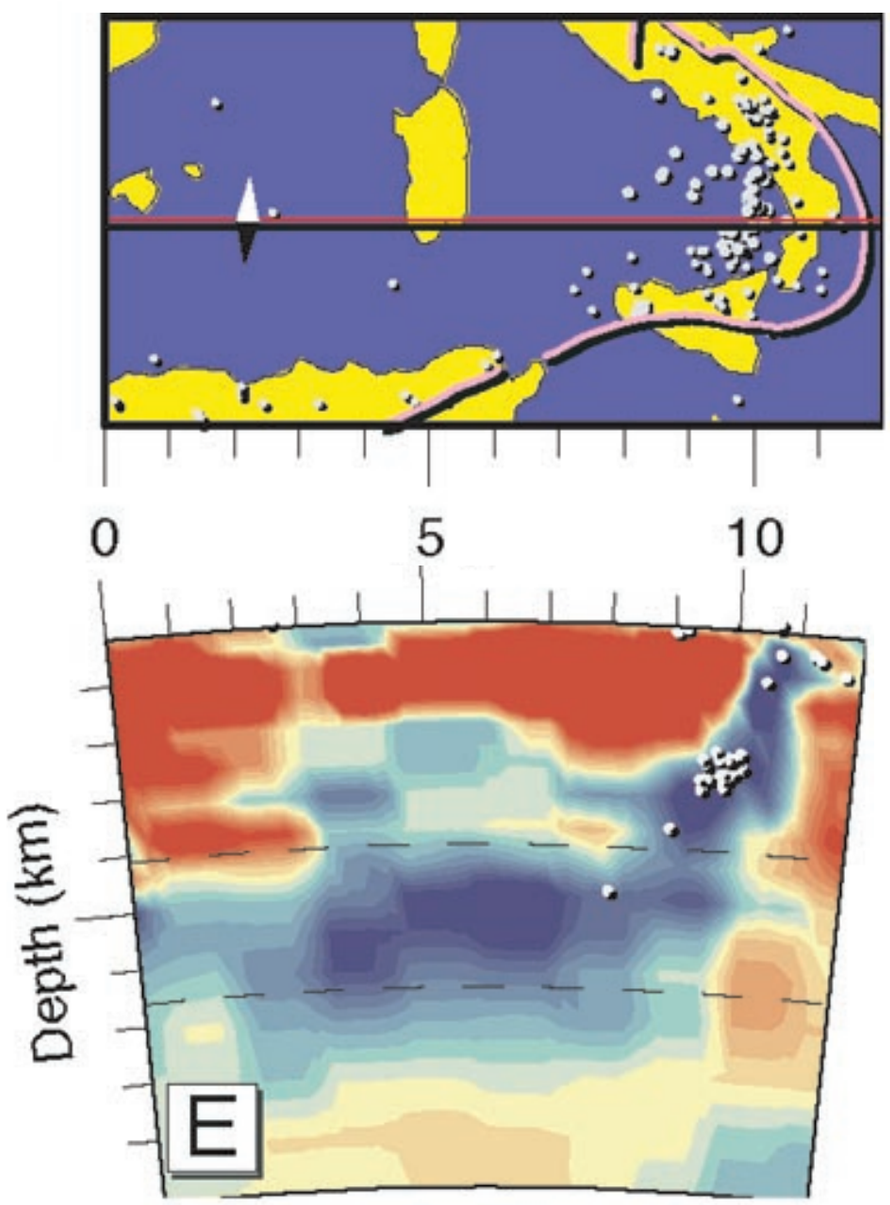

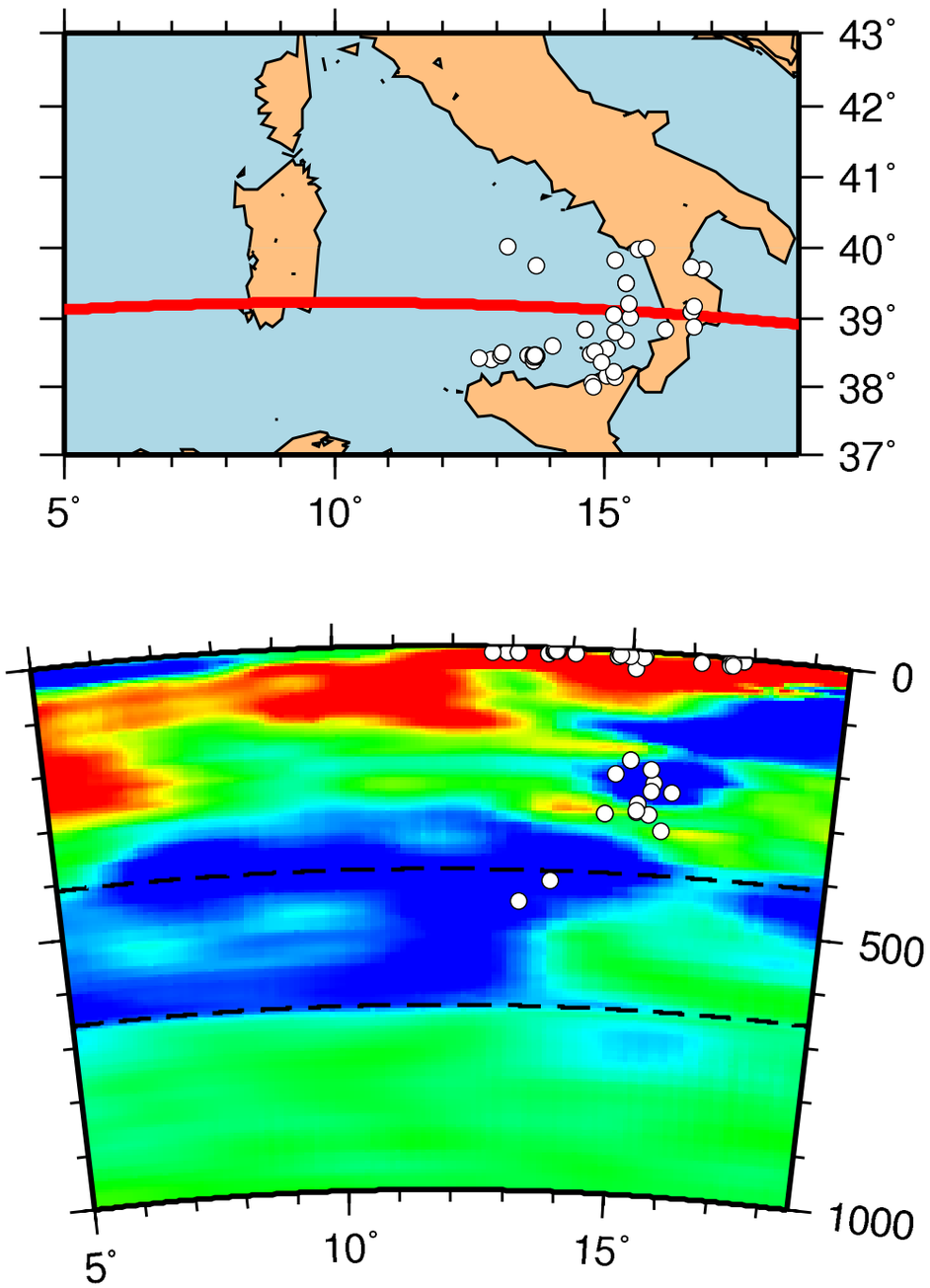

Anisotropy

Depth 75 km